JOINT EUROPEAN TORUS JET

JET–P(93)32

H.P. Summers

Needs for Cross-Sections in Fusion Plasma Research

Needs for Cross-Sections in Fusion Plasma Research

H.P. Summers[1]

JET-Joint Undertaking, Culham Science Centre, OX14 3DB, Abingdon, UK

[1]Department of Physics and Applied Physics, University of Strathclyde, Glasgow

Preprint of a paper to be submitted for publication in
Advances in Atomic, Molecular and Optical Physics
May 1993

A. INTRODUCTION

1. OVERVIEW OF FUSION PLASMA RESEARCH

One would expect fusion reactor design to be concerned principally with the primary reactants and spent fuel, that is the hydrogen and helium isotopes ^{2}D, ^{3}T and ^{4}He, together with ^{7}Li used for tritium breeding. Early plasma experiments conducted in devices of small dimension were however dominated by interaction of the plasma with the walls and the release of impurity species arising from this. In large machines, it was believed such problems would be reduced, but now, even in the Joint European Torus experiment, JET (c.f. Keen et al, 1991) where the toroidal confinement vessel is 1-2 metres in minor radius, it has become evident that impurities sourced from the vessel walls and plasma contact points are hugely influential on plasma behaviour. Thus, the needs of cross-section data for fusion research are clearly focussed on non-fuel as well as fuel species.

The main class of these are the limiting surface species, and the variety under study and the changes in which are most favoured reflect the intense effort in finding materials which can satisfy the engineering demands of the fusion reactor environment. Materials for boundary surfaces, that is limiters, divertors and other first wall components of fusion devices, have to satisfy a number of criteria including high conductivity, high melting and sublimation temperatures, low tritium retention, low sputtering and resistance to chemical release pathways under a reactive plasma loading. These aspects relate mostly to prevention of material ingress into the plasma. Once the material is contaminating the plasma a fresh set of criteria are involved including low radiative losses, small contribution to Z_{eff} and mobility in specific plasma regions such as divertors (see Wesson (1987) for an overview).

The second class of non-fuel species are those which can play a special diagnostic or control role. The spectral emission by impurity ions in plasmas provides probably the most powerful diagnostic insight into the plasma and its behaviour. Controlled injection or introduction of particular species can exploit impurities in an active diagnostically helpful manner. Also, efficiently radiating species influence local plasma temperature through the power balance and so have a plasma control dimension provided they can be appropriately located, for example in divertor chambers. Broadly, therefore, the two classes of impurities with which to be concerned are the *intrinsic* impurities, necessarily present in the plasma because of their use as material components, and the *extrinsic* impurities which are actively introduced.

The evolving route with intrinsic impurities can be illustrated by the situation at the Joint Eurpoean Torus experiment (JET). The first (plasma facing) wall material is Inconel (74% Ni, 16% Cr, 8% Fe) alloy and original plans allowed for restricting the plasma by either carbon or nickel plate limiters. However the dramatic increase in radiated power and plasma disruptions caused by even modest metal influx led to the use only of the carbon limiter.

Subsequent strategy was to minimise plasma contact with metal walls in any circumstances (especially disruptions) by introduction of belt limiters of graphite (carbon fibre reinforced composite), by protection of the inner wall and of all exposed regions such as ribs on the octant sections and radio frequency heating antennae screens, and by depositing carbon generally to depths of a few hundred monolayers by glow discharges in methane mixtures. JET, in these activities, led one school of thought in intrinsic impurities, that is towards lower Z species. From 1989, JET carried out experiments on the use of beryllium as the plasma contacted material (Thomas, 1990). Initially, evaporation of beryllium over exposed surfaces was performed and subsequently a major experiment in which one carbon belt limiter was replaced by one of solid beryllium tiles and with provision of a toroidally complete ring of beryllium tiles at the bottom of the vessel. This latter arrangement is for so called 'divertor-like' operation in which an internal poloidal magnetic null is located within the plasma volume. JET was capable of both carbon or beryllium divertor-like operation at the top or bottom of the vessel respectively (Tanga et al., 1987) allowing comparison of the two species. There is a low Z_{eff} with beryllium, probably due to its 'gettering' action for oxygen and low radiative losses, but severe damage to tiles under heavy power loading. Carbon on the other hand displays the catastrophic growth in impurity flux under high heat loads called the 'carbon bloom' (Jaeckel et al., 1992), which terminates high performance discharges (a controversial issue which may involve β limits). JET is now moving into a next step of construction of a true pumped divertor (Keen et al., 1992)

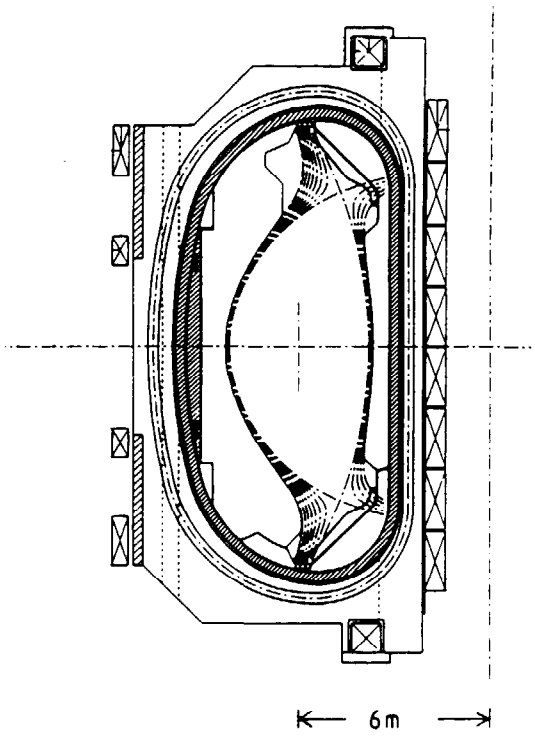

Fig. 1. The International Tokamak Experimental Reactor, ITER design schematic. The divertor, steeply inclined dump plates and magnetic separatrix are shown at the top and bottom of the vacuum vessel (Tombabachi et al., 1991)

which is seen as the way forward for active impurity control. Such design concepts will be incorporated in the planned international tokamak ITER (Tombabechi et al., 1991) (see Fig.1) for which the dump plates and divertor throat materials remain undecided at present between beryllium and carbon.

At other carbon surface based machines, it has proved effective to 'boronise' (for example by discharges in B_3H_7 etc.) giving results similar to beryllium and studies continue on boronised graphite materials (Hirooka et al., 1990). On the other hand, there is a view that because of the rapid erosion of graphitic materials, metal dump plates will eventually be necessary in a practical reactor. So parallel studies take place on the use of high Z metals especially molybdenum (Alcator C-mod) (May et al., 1992) and tungsten in divertors and divertor simulators such as PISCES (Hirooka et al., 1991). It is therefore evident that intrinsic species H, He, Li, Be, B, C, O are of central importance in fusion research together with a number of heavier species of which Si, Ti, Cr, Fe, Ni, Mo, W can be picked out.

Turning to extrinsic impurities for diagnostic purposes, there are four methods, namely beam injection, solid pellet injection, gas puffing and laser ablation, used for introduction of species into the plasma. Diagnostic beams of ^1H, ^2D, ^3T, ^3He, ^4He and ^7Li are used in fusion research, the hydrogen and helium group with strongly bound electrons, in deeply penetrating fast beams for central plasma probing (Summers et al., 1991) and lithium, for the edge plasma (McCormick, 1986). Deuterium pellets are used for deep fuelling but lithium pellets are considered for diagnostics. Metastable rich helium beams have also been suggested as edge probes. Gas puffed species include He, Ne, Ar and occasionally Kr. The choice of laser ablated species is very wide. Fe and Ni are commonly used since already present as intrinsics. Many other heavy species are introduced depending primarily on the central plasma temperature so that the preferred radiating ions of these elements (especially Li-like and Na-like) occur at convenient spatial locations in the plasma for diagnosis. At JET, Ge, Sn and Ag have been used for transport studies by observing transient growth and then decay of their spectral emission.

In assessing the role of impurities and the consequent needs for cross-section data, the fusion plasma divides into three principal regions. The high temperature confined plasma is the familiar region to which most attention has been given historically. It extends from the last closed flux surface approximately to the plasma core with electron temperature, Te, varying from ~100eV to many keV. It might be viewed alternatively as that part of the plasma which can be treated as essentially uniform over closed flux surfaces. In it, the concern is principally confinement and radial diffusion of species. The second region which must be distinguished is plasma penetrated by neutral beams. Neutral beams of $^2D^0$, $^3He^0$ and $^4He^0$ are used for heating the plasma as well as for diagnostic probes. The beams are unique in that they cross the confining magnetic field and provide a source of un-ionised atoms in the high temperature regions of the plasma. They influence impurity ion populations in the penetrated plasma and also, after ionisation, yield a source of fast ions in the plasma. Thirdly there is the edge and

scrape-off-layer plasma (SOL). The SOL is the region outside closed magnetic flux surfaces where particles can stream freely along field lines to solid boundaries (see Stangeby & McCracken (1990) for an overview). It mediates the plasma surface interactions, is central to impurity control and is the primary focus of fusion studies at the present time. Divertors in particular are designed to channel the SOL plasma away from the main plasma chamber to a separate chamber where surface interactions and impurities can be restricted. In addition to these primary regions, there are a number of special environments where the impurity species form distinct populations. Traditionally, electron-ion collisions have received virtually all of the attention in fusion research. In later sections it will be found that nearly equal weight must be given to ion-atom collisions. This is because of the new emphasis on fast neutral beams, likewise, because of the relatively high concentrations of neutral hydrogen which occurs in divertor plasma.

It does appear that two distinct types of usage of atomic data have developed in fusion plasma studies. At one extreme is the use and need of atomic data for large scale plasma modelling, that is for relatively complex numerical magneto hydrodynamic and kinetic equations solutions in which impurities are represented by a few *effective* species. These may be mean charge states at the simplest level or, at a more complete level, the individual charge states of each impurity. They are treated as the dominant populations and only atomic coefficients, such as radiated power, ionisation and recombination for them are considered. At the other extreme, there is diagnostic spectroscopy in which populations of particular excited states of specific ions must be evaluated in detail, with an increase of three or four orders of magnitude in the atomic collision data required. Inevitably, with such large differences in apparent needs, the two areas have tended to become disconnected. However, as fusion conditions are approached and particularly as difficult environments such as divertors are addressed, this separation is unhelpful and has to be prevented. Diagnostic spectroscopy is the cutting edge of validation of atomic processes in fusion plasmas and the use of atomic data in global models must be kept up to date with it. It is a view of this paper that the needs of atomic data for fusion research are only partly for more cross-sections of greater accuracy, but also for attention to the organisation and management of it. Data should be carefully arranged for diagnostic spectroscopic studies so that simplification and condensation to the requirements of global modelling can be performed easily, indeed semi-automatically, so that validity, updating and attribution are ensured. In the next subsection, these connections and requirements are developed.

2. GENERAL ASPECTS OF DATA ORGANISATION AND NEED

a. Dynamical and quasi-static populations. The dominant populations for an elemental species in a plasma are those of the ground and low lying metastable states of each of its ions. They are usually the populations of the lowest terms of each spin system of the ion. This is

because, unlike the situation in very low density astrophysical plasmas, collisional excitation and deexcitation rates of metastables in fusion plasmas exceed radiative decay in most circumstances. Of course, forbidden line radiative transition probabilities vary strongly with ion charge along a given isoelectronic sequence. At low and moderate Z, metastable terms matter, whereas at high Z, the key metastables have to be re-identified with the levels of the ground term. In either case, it remains probable that an ionisation, recombination or excitation event in a fusion plasma may take place from a metastable state. From the point of view of atomic population relaxation timescales, there is a ranking of the form

$$\tau_{meta.} >> \tau_{excit.} >> \tau_{reson.}$$

distinguishing metastable populations, excited states which can freely radiate, and doubly excited states such as occur in delectronic recombination which can autoionise. The situation, in the fusion plasma environments of most interest here, is that plasma dynamical timescales, τ_{plasma}, which may be diffusion times of particles across temperature or density scale lengths or true plasma temporal variation, lie in the vicinity of $\tau_{meta.}$. Excited state populations on the other hand are usually relaxed relative to local metastable populations. Exceptions can be excited populations in beams. Populations can therefore be separated into dynamical populations (metastables) and quasi-static populations (excited states). The former should be included explicitly in global plasma models whereas the latter may be treated in local atomic statistical equilibrium models (von Hellermann & Summers, 1992). Fundamental atomic data should therefore be structured for use in local excited population calculations which can be carried out independently of the plasma models. They prepare (1) the effective source terms for the dynamical populations in plasma equations, particularly effective ionisation, recombination and total power loss coefficients; (2) the populations of excited states and particularly effective emission coefficients for spectral emission obtained as multipliers of the appropriate dynamical populations but evaluated in a quasi-static picture; (3) the supplementary data required for construction of complex observed spectral features.

It should be noted that plasma models which ignore metastables can make significant errors, for example in studies of inflowing divertor species or in dielectronic recombination. Equally a statistical balance assumption for the metastables relative to the ground populations as is done commonly in solar astrophysics or a general assumption of ionisation balance are not necessarily valid in the dynamic regions of interest in fusion plasmas at the present time.

b. The generalised collisional-radiative model. In incorporating atomic reactions into models for high temperature, low density plasmas such as tokamaks, it has been the usual practice to adopt the so called 'coronal approximation' (Seaton, 1964). It is assumed in this picture that collisional excitation takes place only from the ground state of ions and only radiative decay from excited states; also that collisional ionisation is balanced by radiative electron capture (that is radiative and dielectronic recombination). All other collisional

processes are neglected. For the species and environments of interest here, especially the plasma edge and beams this simplification is not justified. Ionisation from excited states, collisional redistribution of population amongst excited states and other mixing processes are of considerable importance. Thus the basis of all modern studies is collisional-radiative theory (Bates et al., 1962), which, must be used in its generalised form (Summers & Hooper, 1983) because of the importance of metastables.

Consider the ions of charge state z, X^{+z} of element X. Let z_0 be the nuclear charge. Denote metastable states by Greek suffices and normal excited states by Roman suffices as X_ρ^{+z} and X_i^{+z} respectively. The rate of transition between states i and j is the sum of a radiative part, $A_{i\to j}$ (if state j is of lower energy than i) and collisional parts $N_e q_{i\to j}^{(e)}$, $N_p q_{i\to j}^{(p)}$, $N_{z_0} q_{i\to j}^{(z_0)}$ etc. due to the major free particles in the plasma. The collisional-radiative matrix, C, denotes these formally as

$$C_{ji} \equiv A_{i\to j} + N_e q_{i\to j}^{(e)} + N_p q_{i\to j}^{(p)} + \ldots. \qquad (1)$$

The rate coefficients $q_{i\to j}^{(e)}$ etc. are usually functions of temperature, Te, Tp, etc. In virtually all circumstances in fusion plasmas, the free electrons may be assumed Maxwellian, but displaced Maxwellians, that is into the rest frame of a moving ion, may be required for ion collisions. With the dynamical and quasi-static assumptions of the previous section, the population equations take the general form

$$\frac{dN_\rho^{(z)}}{dt} = C_{\rho\sigma} N_\sigma^{(z)} + C_{\rho j} N_j^{(z)} + C_{\rho\sigma_+} N_{\sigma+}^{(z+1)} + C_{\rho\sigma_-} N_{\sigma-}^{(z-1)} \qquad (2)$$

$$0 = C_{i\sigma} N_\sigma^{(z)} + C_{ij} N_j^{(z)} + C_{i\sigma_+} N_{\sigma_+}^{(z+1)} + C_{i\sigma_-} N_{\sigma_-}^{(z-1)} \qquad (3)$$

The diagonal elements $C_{\rho\rho}$ and C_{ii} are negative being the total loss rates from the levels ρ and i. There is one such equation for each metastable ρ and excited state i. The $C_{\rho\sigma+}$ and $C_{i\sigma+}$ are recombination rates which may be separated as

$$C_{i\sigma_+} \equiv N_e \alpha_{i\sigma_+}^{(r)} + N_e \alpha_{i\sigma_+}^{(d)} + N_e^2 \alpha_{i\sigma_+}^{(3)} + N_H \alpha_{i\sigma_+}^{(c)} \ldots. \qquad (4)$$

denoting radiative, dielectronic, three body and charge exchange (from ground state neutral hydrogen) parts from each X^{+z+1} metastable. The $C_{\rho\sigma_-}$ are metastable selective direct ionisation rates. The standard procedure is to solve equations 3 for the $N_i^{(z)}$ in terms of the metastable populations. This immediately yields the useful coefficients for spectral studies such as effective emission coefficients. For example, the photon emissivity in the spectrum line i→k may be written as

$$\begin{aligned} \varepsilon_{i\to k} &= A_{i\to k} N_i^{(z)} \\ &\equiv N_e qeff_{i\to k,\sigma}^{(e)} N_\sigma^{(z)} + N_e qeff_{i\to k,\sigma_+}^{(e)} N_{\sigma+}^{(z+1)} + \ldots. \end{aligned} \qquad (5)$$

being composed of electron impact excitation parts, recombination parts etc., associated with each metastable and including all redistributive effects. Eliminating the excited populations

$N_j^{(z)}$ in equations 2 in favour of the metastable populations using equation 3 gives on the right hand side the generalised collisional-radiative source terms for the plasma dynamical equations.

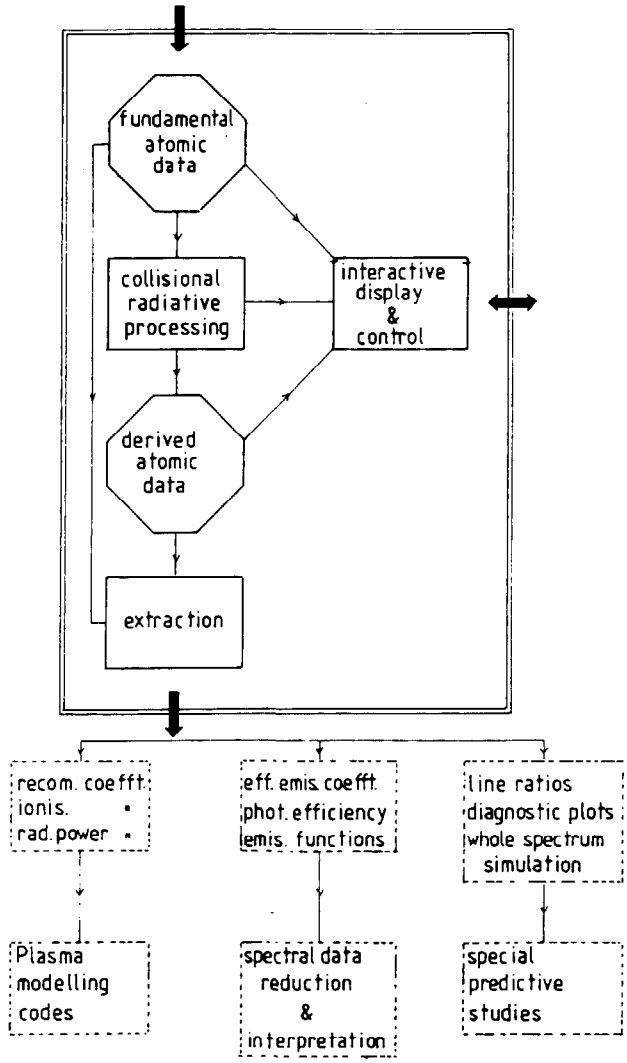

Fig. 2. Schematic of fundamental and derived atomic data organisation and collisional radiative processing. Atomic physics manipulations are a self-contained part within the overall diagnostic/modelling/interpretation loop.

These are usually written in the form

$$\frac{dN_\rho}{dt} = -N_e\left(\sum_{\sigma_+} Scd_{\rho\to\sigma_+} + \sum_{\sigma} Xcd_{\rho\to\sigma} + \sum_{\sigma_-} \alpha cd_{\rho\to\sigma_-}\right)N_\rho^{(z)} \qquad (6)$$

$$+ \quad N_e\sum_{\sigma} Scd_{\sigma_-\to\rho} N_\sigma^{(z-1)} + N_e\sum_{\sigma} Xcd_{\sigma\to\rho} N_\sigma^{(z)} + N_e\sum_{\sigma_+} \alpha cd_{\sigma_+\to\rho} N_{\sigma_+}^{(z+1)}$$

with collisional-radiative ionisation coefficients Scd, cross-coefficients Xcd and recombination coefficients αcd.

The organisation required to support present fusion studies is therefore the preparation and storage of data in a suitable form to generate the collisional-radiative matrix, the manipulation procedures above, the storage of the relevant derived data such as from equations 5 and 6 and the drawing of the derived data into spectroscopic and modelling applications.

Revision of the collisional-radiative matrix data can then be propagated rapidly through the chain. A schematic is shown in figure 2. The important issue for the various regions, species and objectives is to decide the appropriate size for the collisional-radiative matrix, that is, how many levels should be included, whether recombination or charge exchange parts are required and what simplifications are appropriate in the handling of the collisional-radiative equations.

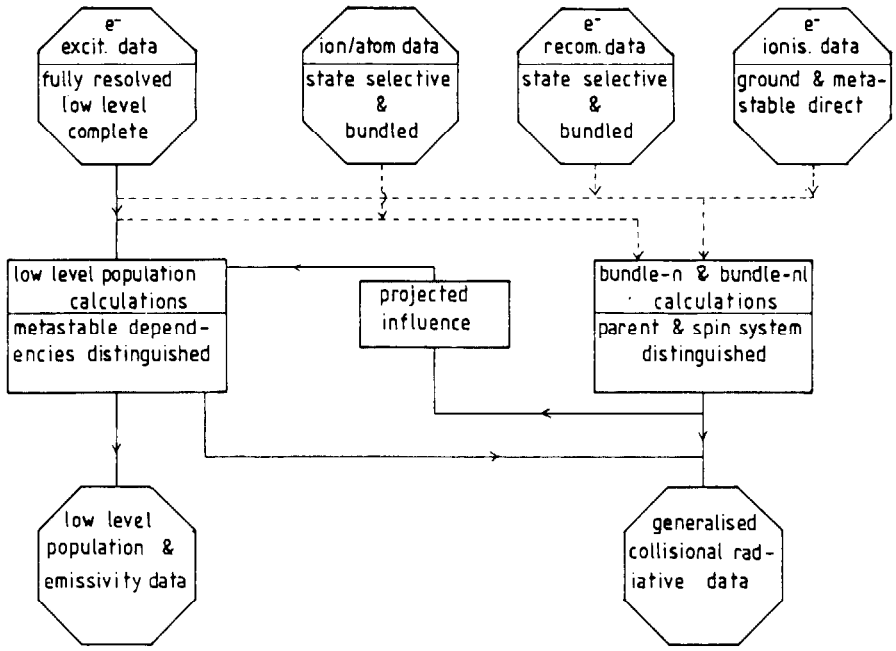

Fig.3. Combination of data sources and collisional-radiative calculations at different resolution levels using condensation methods.

c. Population bundling For a given ion, a low group of principal quantum shells, say $n_0 \leq n \leq n_1$, are identified which include the metastable states and the upper states of observed radiative transitions. The populations of states from these n-shells must be treated in detail in the collisional-radiative calculations. For low charge states, data for separate LS terms, while for high charge states, data for separate LSJ levels are appropriate. This is called the resolution level of the data. In emission from beam atoms, Stark-state resolution is more appropriate than LS- or LSJ-resolution. Higher n-shells $n>n_1$ are less important, also collisional processes become very efficient in redistributing populations of nearly degenerate substates towards statistical. Therefore grouping or bundling together of populations becomes reasonable. In

bundled populations, it is assumed that relative populations of substates are statistical. Progressing to higher n-shells, nl-resolutions and then n-resolution become appropriate with bundle-nl and bundle-n populations respectively (Burgess & Summers, 1976, 1987; Summers, 1977). An integrated strategy on the collisional-radiative matrix includes data at several resolution levels. In practice, full resolution up to n-shells of 4 or 5, nl-resolution up to n-shells ~20 and n-resolution up to n~1000 more than satisfies the needs of general spectroscopy, charge exchange spectroscopy and recombination description.

Atomic modelling calculations at the different resolution levels in isolation are useful for specific kinds of derived data, for example nS-resolution for the generalised collisional-radiative coefficients, αcd. However the most complete studies require linking of the calculations at different resolutions. One simple and convenient method of achieving this is to use the condensation approach as for projecting the influence of excited populations on metastable populations. For example, in a bundled-n calculation, the influence of all the n-shell populations may be condensed into a set of effective collisional radiative coefficients which give the couplings between a specified group of low n-shell populations, $n_0 \leq n \leq n_1$ say. The direct coefficients between the low n-shell populations may be eliminated leaving essentially an indirect collisional-radiative matrix, including recombination and ionisation parts, between the low group of levels, but in bundle-n approximation. This may be expanded using statistical weight arguments over a bundle-nl or fully resolved set of states spanned by $n_0 \leq n \leq n_1$, and combined with the higher precision direct collisional-radiative matrix for them. In this manner the high n-shell influence is maintained in detailed low level studies (Fig. 3) (Summers & Dickson, 1992).

To summarise, organisationally the primary need is for collision data to be assembled together with radiative and energy level data to allow detailed generalised collisional-radiative calculations. Such an organised data set might be called a 'specific ion file'. Specific ion files for spectroscopic studies are required at a high resolution and at high precision, but usually spanning a modest number of n-shells. Lower resolution collisional-radiative calculations spanning very many n-shells must also be supported. Manipulations on the collisional-radiative matrices can then yield all necessary derived quantities for plasma modelling and spectroscopy.

d. Approximate forms. Semi-empirical formulae and algebraically simple expressions have played an important role in making accessible atomic coefficients for fusion modelling. The Burgess general formula for dielectronic recombination (Burgess, 1965), the van Regemorter formula for excitation (van Regemorter, 1962), Lotz expressions for ionisation (for example, Lotz (1967)) and other similar formulae were used enthusiastically and remain deeply embedded with minor adjustments in the plasma modelling codes in many fusion laboratories. Although such formulae may only be accurate to within about a factor three in some cases, they had the special merit that it was relatively easy to obtain some values for virtually every ion of every element

which came under scrutiny. Such accuracies do not satisfy the needs of spectroscopic modelling nor are they sufficient in the approach to ignition in plasma transport modelling .

New collision data for fusion is essentially numerical and is often used directly in that form. However there is much interest in fitting functional forms to data for compactness. Often these are mathematical forms, such as Chebyshev polynomials (for example, Barnett (1990)), but there is a returning trend to more physically based forms with special attention to correct asymptotic behaviour (Burgess & Tully, 1992). Physically reasonable forms with one or two adjustable parameters are called here 'approximate forms' and are of considerable value and importance. The approximate forms may be compact computer algorithms as well as analytic expressions. In practice, numerical cross-section data may have to be repositioned at more convenient energies, extended in range and possibly quadratures performed. Optimising an appropriate approximate form to the numerical data allows the ratio to be used as a slowly varying interpolant and a controlled extrapolant as well as giving immediate visual checks of data error. Also the optimised approximate form and its parameters may substitute the older usages without much structural change. Finally, in the needs for generalised collisional radiative atomic models, it is often found that much data is published and available in unusable added up forms, for example zero density total dielectronic recombination rate coefficients, or final state summed ionisation rate coefficients. Suitable approximate forms optimised to these may allow a tentative subdivision (Summers & Wood, 1988)

In general therefore, as well as a need for numerical collision data, there is need for attention to preparation and recommendation of supporting approximate forms. These are required for all the types of data and some specific aspects will be mentioned briefly in the later sections. In this context, it should finally be noted that most collisional-radiative modelling codes establish a complete basis of atomic data for the collisional-radiative matrices using simpler approximations first and then substitute selectively with best available data.

e. Accuracy requirements. In general in fusion plasmas experiments, absolute intensity calibrated measurements of spectrum line emission rarely have uncertainties less than ~30%. This is due to reasons such as window transmission changes in situ, uncertain alignment shifts during operation, etc. Often the situation is much worse. Relative calibration is however usually better and so close-lying line ratios are known to higher accuracy. Broadly an appropriate accuracy for calculated populations emitting measured lines may be set at ~20%, this figure being that also of the principal excitation rate coefficients contributing to these populations.

In time dependent ionisation studies, the precision of fitting the occurrence of ionisation state time histories indicates that an ionisation coefficient shift of 20% is not detectable. Similarly sensitivity studies on plasma impurity radial diffusion models suggest accuracies of this order for ionisation and recombination coefficients to avoid interpretation of errors in these

coefficients spuriously as changes in apparent diffusion coefficients. Thus 20% is a reasonable bound on the key fundamental collisional rate coefficients for application in fusion. The exception is in beam attenuation cross-sections where a much higher accuracy, typically ~5-10% is necessary. Accuracies required of contributions to composite coefficients are pro rata.

B THE CONFINED HIGH TEMPERATURE PLASMA

The picture of this region is of nested toroidal closed magnetic flux surfaces, on which the magnetic field lines are helical, extending from the last closed flux surface to the plasma centre. This configuration, together with the associated safety factor q of each flux surface, where $q \approx r.B_{tor}/R_0.B_{pol}$ (r is the minor radius of the flux surface and R_0 is the plasma major radius), is designed to provide the stable thermally insulated core plasma in which energy confinement time, density and temperature can approach the fusion ignition requirement $\tau_c n_c T_c \sim 5x10^{21} m^{-3} s$ keV. Thermal conduction, radiant energy losses and particle diffusion or convection radially, that is across flux surfaces, are the key parameters. It is evident that the radial transport of energy and particles in tokamaks is anomalous (Wesson, 1987). In addition this transport can be altered in certain operational modes. In particular, in X-point configurations, when there is a poloidal magnetic field null at the top and/or bottom of the vessel within the plasma volume and non-ohmic neutral beam or radio frequency heating is above some threshold value, enhanced confinement (over normal 'L-mode') called 'H-mode' occurs (Wagner, et al., 1982; Tanga et al., 1987). Also periodic and non-poloidally symmetric disturbances occur such as m=1 relaxation oscillations ('sawteeth') associated with the q=1 surface, and edge localised instabilities ('ELMS' causing H-mode to L-mode transitions) near the last closed flux surface (Burrell et al., 1989). These are important matters bearing upon sustained achievement of high temperatures, controlled high confinement, release of fusion ash, impurity accumulation in the plasma core and so on.

Impurities directly affect the energy balance through their contribution to radiant energy losses (McWhirter & Summers, 1984; Post et al., 1977) and to Z_{eff} which determines ohmic energy input and the current profile. Also their contribution through ionisation to the free electron density modifies deuterium/tritium fuel concentration. Secondly, partially ionised impurities can act as key markers of the diffusion and transport processes by observation of the distribution of their spectral emission spatially and in time. Finally spectral line combinations of a number of ion types allow diagnostic insights into ion and electron temperatures, electron density, dilution and dynamic states of ionisation in fusion plasmas.

Diffusive studies are usually based on matching families of solutions of the one-dimensional radial number density continuity equation for the ions of an impurity element with observation (Behringer, 1987; Hulse, 1983; Michelis & Mattioli et al., 1984; Stratton et al.,

1987). The parameters of the solutions are the diffusion coefficient D and the inward convective velocity v of the flux $\Gamma^{(z)}$ of ion X^{+z} described in the form

$$\Gamma^{(z)} = D\frac{\partial N^{(z)}}{\partial r} + v\,N^{(z)} \qquad (7)$$

v essentially determines the central peakedness of the impurity density and D the width of ionisation stage radial profiles. Most observations are of a number of VUV and XUV resonance spectrum lines from a range of ionisation stages of each element integrated along a radial line of sight through the centre of the plasma. The absolute calibration has quite high uncertainties. There are relatively few systematically observed radial emission profiles from Abel inverted multichord data. Also for intrinsic light impurities, ionisation to the bare nucleus occurs not far from the last closed flux surface in typical discharges. Thus it is relatively difficult to deduce D and v and especially their radial variation which may be marked in H-mode (Giannella et al., 1989). Mapping of the time evolution of emission from ionisation stages of laser ablated heavier species is a useful approach (Pasini et al., 1990). However it is evident that, to prevent misinterpretation, proper attention must be given to the ionisation and recombination coefficients which are the source terms in the right-hand side of the continuity equation. The precisions of Section A.2.e. in atomic data are apposite and this requires the sophistication of Section A.2. The availability of such data is far from complete for the range of ablated impurities in use or likely to be used. Absolute impurity concentrations and then total radiated power are often sought from a concensus of a few individual lines measured spectroscopically and various wavelength integrated measurements such as in the X-ray region and bolometry (Lawson and Peacock, 1992). These cannot be represented to adequate accuracy by the coronal, dipole only, no cascade or redistributive corrected theoretical approximations. A more detailed assessment of the appropriate parts of the collisional-radiative matrix is required and this would parallel a trend towards complete simulation and matching of survey spectrometer observations.

For spectral diagnostics of high temperature plasmas, it is above all the helium-like lines and the associated satellite lines which have received attention. Also they are important contributors to integrated and partially energy resolved measurements such as pulse height analysis (Pasini et al., 1988). In a plasma, the occurrence of the helium-like ion of an element is the most spatially extended, because of its high ionisation potential, while the high first excitation energy determines that its spectrum is influenced by recombination. Deduction of central plasma ion temperature from the resonance line (w) together with inference of whether the ionisation is in equilibrium are the main objectives, the analysis usually using spectral synthesis and matching techniques (Bitter et al., 1985; Bombarda et al.,1988). As plasma core temperatures increase, selection of heavier probe species is necessary. The intrinsic species nickel at JET, in higher temperature discharges, has its NiXXVII radiation shell well off-axis where differential rotation and the path of line of sight integrals complicate interpretation (Zastrow et al., 1990; Danielsson et al., 1992). Also results have to be related to central plasma by ionisation balance arguments. Uncertainties do persist in whether the ionisation is

stationary and in line ratios such as x/y, probably stemming from the collision cross-section data (Bitter et al., 1991). It does appear however that the diagnostic return from helium-like ions, as distinct from the fundamental physics return with the fusion plasma merely as a well specified light source, is modest for the effort which has gone into them. The quality of spatially resolved electron temperature and density measurements of the confined plasma using active techniques such as scattering of laser light (LIDAR) (Gowers, 1991) and electron cyclotron emission (ECE)

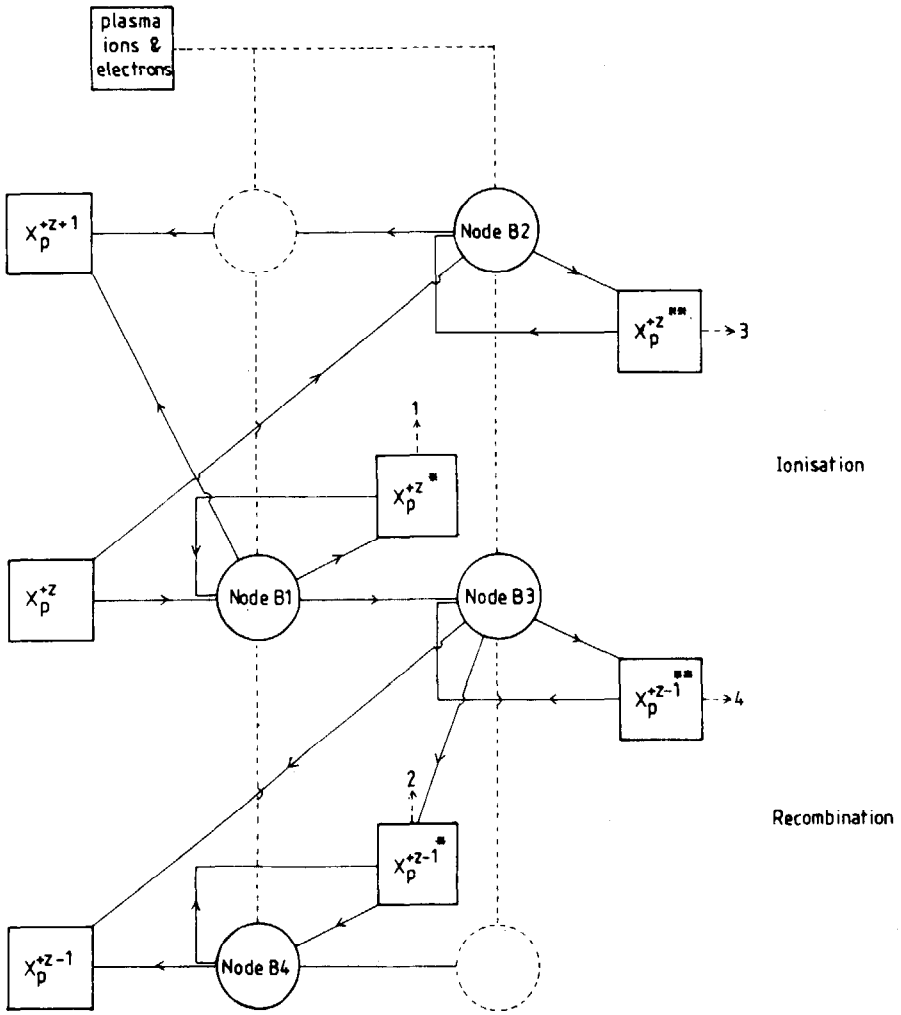

Fig. 4. Working diagram of populations and reaction nodes for the ionisation, excitation and recombination of ions in high temperature confined plasmas.

(Costley, 1991) (see also Stott (1992) for an overview) mean that spectral diagnostics with probe species are only relevant for more elusive plasma parameters.

There are some such opportunities in for example higher members of the boron-like (Sato et al., 1987) and fluorine-line (Keenan & Reid, 1989) isoelectonic sequences where ground term fine structure level populations are partially mixed by deuteron collisions and the forbidden lines are observable (Denne et al., 1989) . Spectral line ratios here relate to deuterium dilution and

deuterium temperature (Summers et al., 1990). Extension of the atomic collision database, including positive ion collisions as well as electron collisions allows exploration of such possibilities in the fusion plasma domain.

For assembling the necessary collision cross-section and radiative data, a working diagram for excitation, ionisation and recombination for the confined plasma is shown in Fig. 4. The key populations are represented by square boxes and the reaction nodes by circles. Numbered populations give rise to observed features which are illustrated in later figures. These features are cross-referenced by the notation [working diagram number . population number]. Also to be noted are the re-entrant loops which indicate collisional-radiative calculations involving excited states (*) and doubly excited states (**). The capital letters indicate representative observable features which are illustrated in the associated figures 5 and 6. The importance of reactions are indicated approximately by symbols (#1) [most important, accuracy ≤10%], (#2) [10-25%], (#3)[25-50%], [#4)[50-75%], (#5)[least important >75%]. Fig. 4 is organised to show the pathways for excitation and ionisation from ion X_p^{+z} to X_p^{+z+1} and then the pathways for recombination and cascade from X_p^{+z} *to* X_p^{+z-1}. In reality both pathway sets occur for each ion pair. The subscript p denotes a plasma ion with a thermal Maxwellian velocity distribution function.

1. EXCITATION AND IONISATION

Node B1 represents processes connecting the metastables ρ of ion X_p^{+z} with its excited states and direct ionisation. The primary excitations are by electron collision

$$\begin{aligned} &\text{(\#2)} \quad X_p^{+z}(\rho) + e \rightarrow X_p^{+z}(\sigma) + e \\ &\text{(\#2)} \quad X_p^{+z}(\rho) + e \rightarrow X_p^{+z}((\rho_+)n\ell SL) + e \qquad n_\rho \le n \le n_\rho + 1 \end{aligned} \tag{8}$$

where n_ρ is the shell from which an electron is promoted in metastable ρ. LS coupling is shown and this is relevant for z≤12 after which intermediate coupling denoted by ρ_J and LSJ is necessary. The relevant metastables ρ and ρ_+ for the first period isoelectronic sequences are the ground states except for HeI-seq($1s^2\ ^1S$, $1s2s\ ^3S$, $1s2s\ ^1S$), BeI-seq($2s^2\ ^1S$, $2s2p\ ^3P$) BI-seq($2s^22p\ ^2P$, $2s2p^2\ ^4P$), CI-seq($2s^22p^2\ ^3P$, $2s^22p^2\ ^1D$, $2s^22p^2\ ^1S$, $2s2p^3\ ^5S$), NI-seq($2s^22p^3\ ^4S$, $2s^22p^3\ ^2D$, $2s^22p^3\ ^2S$), OI-seq($2s^22p^4\ ^3P$, $2s^22p^4\ ^1D$, $2s^22p^4\ ^1S$), NeI-seq($2s^22p^6\ ^1S$, $2s^22p^53s\ ^3S$) and similarly for the second period but with increasing complexity due to 3d orbitals. It is necessary to include non-dipole as well as dipole excitations since, exciting from n_ρ=2 shells, dipole dominance is not assured and all contribute ultimately to the radiated power. Excitation to at least $n=n_\rho+1$ is necessary for the accuracy sought here and has been an omission in much

work. The spin changing transitions are also required since these establish the connections between metastable populations . The direct ionisations are

$$(\#2)\quad X_p^{+z}(\rho\ ) + e \rightarrow X_p^{+z+1}(\rho_+) + e + e \tag{9}$$

where it is necessary to resolve the initial and final metastables ρ and ρ_+. The main redistributive reactions are

$$(\#3)\quad X_p^{+z}((\rho_+)n\ell SL) + e \rightarrow X_p^{+z}((\sigma_+)n'\ \ell'\ S'\ L') + e \quad n_\rho \le n \le n_\rho + 1 \tag{10}$$

The redistributive collisions become less important at high z due to the relative scaling of spontaneous transition probabilities and collisional rate coefficients (z^4 and z^{-3} respectively). However the spin changing transitions (10) are important for depopulating metastables even in the heavier highly ionised elements. The additional ionisations from excited states are

$$(\#3)\quad X_p^{+z}((\rho_+)n\ell SL) + e \rightarrow X_p^{+z+1}(\rho_+) + e + e \qquad n_\rho \le n \le n_\rho + 1 \tag{11}$$

where parent changing can be ignored. At higher z, in intermediate coupling, positive ion impact redistributive collisions are important for diagnostics described earlier in this section.

$$(\#4)\quad X_p^{+z}(\rho_J) + D_p^+ \rightarrow X_p^{+z}(\rho_{J'}) + D_p^+ \tag{12}$$

with possible influence of other positive ions besides deuterons. These reactions, together with the radiative transition probabilities allow realistic line intensity calculation and energy distribution of radiated power for the light elements through a collisional radiative calculation. It can be improved however for the light ions by including higher transitions in which lower resolution levels, that is bundle-n and bundle-nℓ, are appropriate

$$\begin{aligned}
&(\#4)\quad X^{+z}(\rho) + e \rightarrow X^{+z}((\rho_+)n[\ell]) + e \\
&(\#5)\ X^{+z}((\rho_+)n[\ell]) + e, D_p^+ \rightarrow X^{+z}((\rho_+)n'[\ell']) + e, D_p^+ \qquad n_\rho + 1 < n, n' \\
&(\#5)\quad X^{+z}((\rho_+)n[\ell]) + e \rightarrow X^{+z+1}(\rho_+)\ + e + e
\end{aligned} \tag{13}$$

The contribution to the radiant power, low level line intensities and effective ionisation at fusion plasma densities fall rapidly with increasing n. However the data required for the generalised collisional radiative ionisation coefficients are still incomplete. In this work we view excited states obtained by adding an electron to a metastable parent as 'singly excited' associated with node B1. However with metastable parents other than the lowest, autoionisation is possible for $n>n_c$ say

$$(\#3)\quad X^{+z}((\rho_+)n[\ell SL]) \rightarrow X^{+z+1}(\sigma_+) + e \quad n > n_c \tag{14}$$

Note that in practice, intermediate coupling calculations may be necessary to obtain all the final states σ_+.

Node B2 represents reactions relating to doubly excited states which can autoionise. The excitation to autoionising levels is an important part of the ionisation pathway for metastable states

$$(\#2)\quad X^{+z}(\rho) + e \rightarrow X^{+z}((\rho_+^*)n[\ell SL]) + e \quad n > n_c \tag{15}$$

where ρ_+^* is an excited parent state and $n>n_c$ again symbolises the opening of the Auger channels. Since the final state matters, the Auger branching to the various final parents must be followed

$$(\#3)\quad X^{+z}((\rho_+^*)n[\ell SL]) \rightarrow X^{+z+1}(\rho_+) + e \tag{16}$$

It is usually assumed that the Auger process occurs promptly. However in principle collisional and field redistribution can interfere. This is represented by the collisional-radiative re-entrant loop at node B2. However this is most significant for recombination and is discussed further there.

2. RECOMBINATION AND CASCADE

Node B3 represents the recombination reactions from X_p^{+z} to X_p^{+z-1}. These include dielectronic recombination and are therefore associated with doubly excited autoionising populations X_p^{+z-1**}. The radiative recombination reactions populate directly metastables and metastable parent based excited states of X_p^{+z-1}

$$\begin{aligned}
&(\#2)\quad X_p^{+z}(\rho_+) + e \rightarrow X_p^{+z-1}(\rho) + h\tilde{\nu} \\
&(\#3)\quad X_p^{+z}(\rho_+) + e \rightarrow X_p^{+z-1}((\rho_+)n\ell SL) + h\tilde{\nu} \qquad n_\rho \le n \le n_\rho+1,\ l \le 2 \\
&(\#4)\quad X_p^{+z}(\rho_+) + e \rightarrow X_p^{+z-1}((\rho_+)n[\ell]) + h\tilde{\nu}
\end{aligned} \tag{17}$$

It is not necessary to consider interference between radiative and dielectronic recombination. Bundled coefficients are sufficient for higher n shells. Three body recombination is of little importance in the high temperature confined plasma, but is obtained as the inverse of the ionising reactions in (9), (11) and (13). The major problem lies with dielectronic recombination since it excites the initial state (parent state) ρ_+ opening up the possibility of branching to different parents in the recombination system. The first reactions are the resonance captures

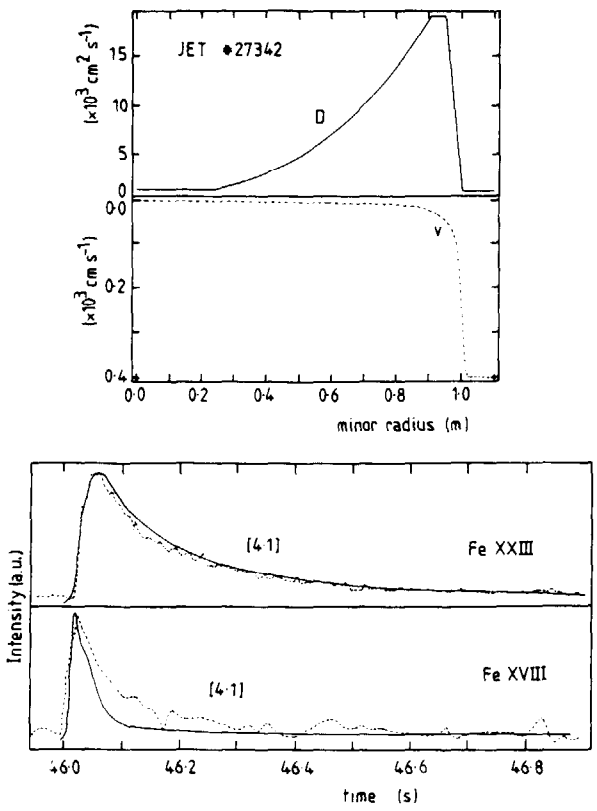

Fig. 5. Normalised time histories of some spectrum lines of Fe during a JET laser ablation study compared with the calculated time histories from a one-dimensional radial transport code. The best match is achieved with a diffusion coefficient which is much smaller in the region r<1.0m. This is characteristic of H-mode. (Denne-Hinnov et al., 1993)

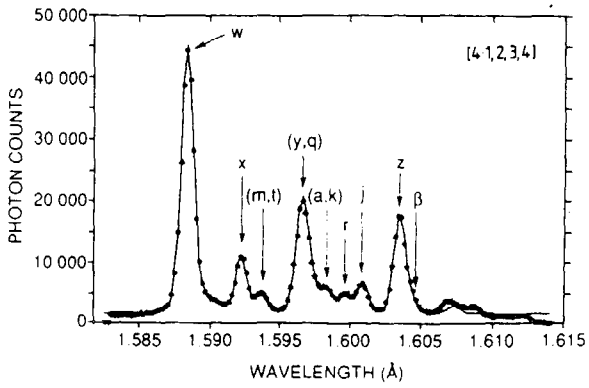

Fig. 6. Matching of observed and synthesised NiXXVII resonance intersystem and satellite lines in a TFTR discharge. The matching yields values for electron temperature, electron density and the ratios of the H-like, He-like and Li-like stage abundances averaged for the line of sight. Deduction of local values requires further information on radial distributions. (Bitter et al.,1991)

$$(\#2)\quad X_p^{+z}(\rho_+) + e \rightarrow X_p^{+z-1}((\rho_+^*)n\ell SL)$$

$$(\#3)\quad X_p^{+z}(\rho_+) + e \rightarrow X_p^{+z-1}((\rho_+^*)\, n[\ell]) \qquad n_c < n \qquad (18)$$

It has usually been assumed that there is no redistribution of the doubly excited states so that reactions (18) are followed by the Auger inverse processes

$$(\#2)\quad X_p^{+z-1}((\rho_+^*)nSL) \rightarrow X_p^{+z}(\sigma_+) + e$$

$$(\#3)\quad X_p^{+z-1}((\rho_+^*)n[\ell]) \rightarrow X_p^{+z}(\sigma_+) + e \qquad (19)$$

or stabilise radiatively

$$(\#2)\quad X_p^{+z-1}((\rho_+^*)n\ell SL) \rightarrow X_p^{+z-1}((\sigma_+)n\ell SL) + h\nu$$

$$(\#3)\quad X_p^{+z-1}((\rho_+^*)n[\ell]) \rightarrow X_p^{+z-1}((\sigma_+)n[\ell]) + h\nu \qquad (20)$$

where all the radiative and Auger paths are included. The doubly excited states can be redistributed by plasma microfields, motional Lorentz electric fields and collisions. The effect in all cases is a redistribution of population to higher ℓ's which enhances the possibility of stabilisation. Recombining lithium-like ions are probably the most vulnerable. In practical terms, the enhancement which can be quite large is always countered by the collisional ionisation processes from excited states (11) and (13) with the resultant effect ≤40% at most. However comprehensive integrated and field mixing studies are difficult. In particular the choice of basis, namely spherical or Stark, and formation of proper averages for isotropic Maxwellian ions requires development in techniques The additional reactions establishing the doubly excited populations can be summarised as

$$(\#5)\quad X_p^{+z-1}((\rho_+^*)n[\ell SL]) + e, D_p^+ \rightarrow X_p^{+z-1}((\rho_+^*)n'[\ell' S' L']) + e, D_p^+$$

$$(\#5)\quad X_p^{+z-1}((\rho_+^*)n[\ell SL]) \xrightarrow{E-field} X_p^{+z-1}((\rho_+^*)n[\ell' S' L']) \qquad (21)$$

where the simplification of ignoring redistribution to other n-shells is appropriate. The direct ionisation losses are

$$(\#5)\quad X^{+z-1}((\rho_+^*)n[\ell SL]) + e \rightarrow X_p^{+z}(\rho_+) + e + e \qquad (22)$$

which ultimately dominate at very high n-shell, merging the bound and free electron population distributions.

At node B4. the radiative recombinations and dielectronic stabilisations (20) enter the singly excited state population reactions. These processes are the same as for the ionisation case at node B1, however the range of n-shells which must be included is greatly increased. Dielectronic stabilisation leads to population of very high n-shells which contribute significantly to generalised collisional-radiative coefficients. Thus the precision of the second and third reactions of (13) must be increased to (#3). Much calculation is done with bundle-n treatment above n_ρ+1. nℓ-resolution up to n~7 is more than adequate for most purposes in fusion since at low z, redistributive collisions establish relative statistical populations by about this n-shell, while at high z, dielectronic recombination decreases and concentrates to lower n-shells so the treatment of the higher n-shells can again be simplified.

C NEUTRAL BEAMS AND BEAM PENETRATED PLASMA

Neutral beams are used to supplement the ohmic heating of tokamak fusion plasmas. Isotopes of hydrogen, especially $^2D^0$ are the most common beam species. The beam particle energies are chosen so that ionisation and therefore energy deposition is principally in the core of the plasma. In present large devices with densities ~$5x10^{13}$ cm^{-3} in the core and minor radii ~1m, for a D(1s) beam, the relevant energies are 40-80 keV/amu. For a machine such as ITER, at densities >10^{14} cm^{-3} and minor radius ~2.5m, substantially higher energies are required to penetrate to the core. Heating beam injectors in use at the present time operate by positive ion acceleration followed by neutralisation in the neutral gas of the same species. For hydrogen isotopes, D, $D_2^+$and D_3^+ species are produced in the injector giving full, half and third energy fractions in the final neutral beam. At entry into the JET plasma, the fractions by power in ^2D injection are 80%:14%:6% typically - a good figure. For operation with $^1H^0$ or $^3T^0$, the $^2D^0$ energies must be scaled by the charge to mass ratio. Thus the relevant beam energies extend to 7-160 keV/amu. An injector assembly may have several individual injectors giving a beam at a slightly different inclination. For JET, the half-width (Gaussian) of each individual beam at the plasma entry is ~20cm and they can be switched on and off individually. Heating beam injection of ^3He and ^4He is also practised, partly to take advantage of deeper penetration (since the electron binding energy for He($1s^2$) is higher than for H(1s)) at higher densities, but also to limit neutron production (cf. ^3He + ^2D and ^2D + ^2D reactions). Helium beams have a metastable content (1s2s ^1S and 1s2s ^3S) on entry into the plasma, believed to be ≤7% but the subject of some discussion (Gilbody et al., 1971; McCullough et al., 1978; Tobita et al., 1990; Hemsworth and Traynor, 1990;, Hoekstra et al., 1991). There is only a single beam energy fraction with helium beams. Higher energy H^- acceleration beams are under development and will also be mono-energetic. From a plasma physics point of view precise knowledge of beam particle and energy deposition is required. Therefore the first need is for accurate attenuation cross-sections.

The most striking development with neutral beams has been the diagnostic impact, especially on spectroscopic methods. This diagnostic development has mostly made use of the powerful heating beams but also dedicated diagnostic beams particularly for edge plasmas. Firstly hydrogen or helium atoms in penetrating beams are efficient charge exchange donors to impurity ions in the plasma core. This is of particular relevance to light species such as H, He, Be, C, O etc., which are fully ionised in the core. The charge exchange reaction populates preferentially dominant principal quantum shells n ~ $z_0^{3/4}$ where z_0 is the impurity nuclear charge, but with significant subdominant population to $2z_0^{3/4}$. Cascade spectral emission from XUV to visible results (Isler, 1981) which is diagnostic of impurity temperature (Fonck et al., 1983), impurity density (Boileau et al., 1989a), plasma rotation (Groebner et al., 1983) etc. Such

studies are called 'charge exchange spectroscopy'. It is usually carried out at visible wavelengths where intensity calibration is more routine and allows absolute, local measurements of densities. That is provided the beam attenuation at the observed volume is known with precision and the complexity of modelling subdominant receiver populations can be handled satisfactorily. Also it has to be noted that observationally, the broad charge exchange spectrum lines from the plasma core are generally overlapped by narrower emission from the plasma periphery whose separation, by multi-Gaussian fitting reduces experimental accuracy. The most complete studies are with D^0 beams, while the He^0 case is still in development. The attenuation of He^0 is more complex than that of D^0 due to double loss processes but this includes a double charge transfer reaction with He^{+2} in the plasma and so allows external neutral particle detection (Summers et al., 1992c). Secondly the beam atoms themselves are excited and radiate. For D^0 beams, the emission for example in $D\alpha$ is highly perturbed by the motional Stark field (~100kV/cm at JET giving Stark multiplet component separations ~1-2 Å) (Boileau et al., 1989b). The opportunity afforded by this new 'beam emission spectroscopy' is very important. It is diagnostic of internal magnetic fields and plasma ion densities (since ion cross-sections exceed electron cross-sections for such fast beams) as well as allowing measurement of attenuation (Mandl et al., 1993; Wroblewski et al., 1990). It is also proving a probe for density fluctuations (Paul and Fonck, 1990). He beam emission is observed on both singlet and triplet sides (Summers et al., 1991). Although there are some indications of Stark features, they are much weaker than in D^0. This is because the n=4 shell which experiences linear Stark effect is strongly depopulated through the ^1P level to ground so radiating principally in the VUV. The singlet-triplet ratio distinguishes ion and electron collisions and is affected by spin system breakdown. The Stark field influences this through shifts in level coincidences. For D^0 beams at energies ≥20keV/amu, the ground state $1s^2S$ is the principal donor population. At lower energies the excited states contribute to subdominate level population. For He^0 beams, the situation at this stage is less clear. For charge exchange with He^{+2}, the capture to the n=4 shell may be substantially lower than in the D^0 beam case and donation from the 1s2s ^1S and 1s2s ^3S metastables dominant. The atomic collision data need is large in this area and clearly beam emission and charge exchange spectroscopies must be modelled and carried out together.

The principal edge probe beam up to this time has been $^7Li^0$ although Na beams and composite beams including Li and Na have been proposed as differential probes. Metastable rich helium beams have also been suggested. The Li beam energies are ≤9keV/amu typically and attentuate rapidly through the scrape-off-layer (~10cm. decay length for electron density ~ 2.0×10^{13} cm^{-3}). Since electron collisions dominate, the attenuation, as measured by the 2s ^2S - 2p ^2P resonance line, allows reconstruction of the electron density profile primarily (Aumayr et al., 1992). A composite beam with markedly different ionisation potentials would also yield electron temperature. The Li^0 also acts as a charge exchange donor to impurity species allowing

charge exchange spectroscopy (Schorn et al., 1991). Measurement of the polarisation of the π component of the resonance line has also been used to obtain internal magnetic field orientation (McCormick, 1986).

Finally, it should be noted that beams have a set of other populations associated with them, namely plumes and haloes (Fonck et al., 1984). These are the recombined ions and atoms respectively following charge transfer with beam atoms. They can initiate further reactions and must be considered together with the beam atoms. A more detailed specification of the cross-section needs is given in the following subsections.

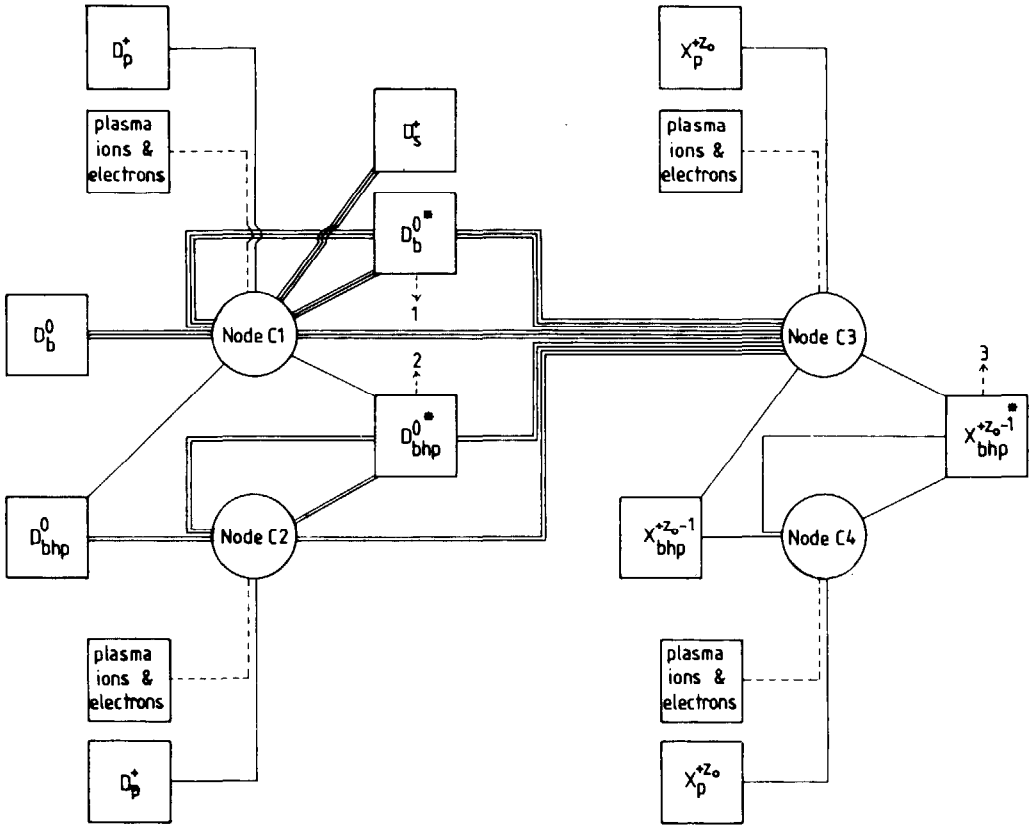

Fig.7. The working diagram of populations and reaction nodes for beam emission spectroscopy and charge exchange spectroscopy using neutral deuterium beams.

1. BEAM ATTENUATION AND BEAM EMISSION

a. Deuterium beams. Although we refer to deuterium in this section, there is no loss of generality in application to other hydrogen isotopes. The working diagram is shown in figure 7. The capital letters indicate observable features illustrated in figures 8 and 9. Beam species have a subscript (b) and plasma species subscript (p). The special plasma populations associated with the beam are collectively called the beam halo plasma and given the subscript (bhp). We shall also use this for impurity populations following charge transfer with the beams although when ions, the term 'plume' is more common.

Node C1 represents the attenuation reactions of the three fractional energy components of the D_b^o beams. The primary reactions are the direct ionisation and charge exchange losses from the ground state by plasma deuteron, other plasma light impurity nuclei and electron collisions.

$$
\begin{aligned}
&(\#1)\ D_b^o(1s)+D_p^+ \rightarrow D_{sb}^+ + D_p^+ + e && 10 \le \text{E/amu} \le 200\text{keV} \\
&(\#1)\ D_b^o(1s)+D_p^+ \rightarrow D_{sb}^+ + D_{bhp} && 0 \le \text{E/amu} \le 200\text{keV} \\
&(\#1)\ D_b^o(1s)+X_p^{+z_o} \rightarrow D_{sb}^+ + X_p^{+z_o} + e && 10 \le \text{E/amu} \le 200\text{keV} \\
&(\#1)\ D_b^o(1s)+X_p^{+z_o} \rightarrow D_{sb}^+ + X_{bhp}^{+z_o-1} && 0 \le \text{E/amu} \le 200\text{keV} \\
&(\#1)\ D_b^o(1s)+e \rightarrow D_{sb}^+ + e + e && 1\text{keV} \le T_e \le 15\text{keV}
\end{aligned}
\qquad (23)
$$

Note that ionisation of a beam deuterium atom leaves a fast D^+ ion which subsequently slows down. We denote the slowing population by subscript (sb). The high energy limit is set approximately by the maximum relative collision energy of up to 100keV/amu beam atoms and 40keV deuterium plasma temperature. The low energy extension is designed to include also the needs for D_{bhp} attenuation (see node C2). The ion impact ionisation cross-sections become small at low energies and the charge exchange cross-sections at high energy. The latter at energies up to 200keV/amu remain relevant for charge exchange spectroscopy, although it is only the total charge transfer cross-sections which are required here. The relevant ions X^{+z_o} are the light element list. Electron collisions contribute up to ~10% at beam energies ≥ 20keV/amu but are progressively more important at lower energies (see node C2). These data alone provide beam attenuation coefficients at zero density where there is no indirect losses via excited states. Excited states must be included at plasma densities $\geq 10^{14}$ cm^{-3} and generally for the study of the beam emission spectrum. The necessary reactions to establish the D_b^{o*} populations and the stepwise losses are ground state excitation,

$$
\begin{aligned}
&(\#2)\ D_b^o(1s)+D_p^+ \rightarrow D_b^o(nkm)+D_p^+ && 0 \le \text{E/amu} \le 200\text{keV} \\
&(\#2)\ D_b^o(1s)+X^{+z_o} \rightarrow D_b^o(nkm)+X_p^{+z_o} && 0 \le \text{E/amu} \le 200\text{keV} \\
&(\#2)\ D_b^o(1s)+e \rightarrow D_b^o(nkm)+e && 1\text{keV} \le T_e \le 15\text{keV}
\end{aligned}
\qquad (24)
$$

redistribution, ionisation and charge exchange from excited states

$$
\begin{aligned}
&(\#3)\ D_b^o(nkm)+D_p^+, X^{+z_o}, e \rightarrow D_b^o(n'k'm')+D_p^+, X^{+z_o}, e \\
&(\#3)\ D_b^o(nkm)+D_p^+, X^{+z_o}, e \rightarrow D_{sb}^+ + D_p^+, X^{+z_o}, e + e \\
&(\#3)\ D_b^o(nkm)+D_p^+, X^{+z_o} \rightarrow D_{sb}^+ + D_{bhp}^o, X_{bhp}^{+z_o-1}
\end{aligned}
\qquad (25)
$$

The energy ranges are the same. The Stark picture is appropriate for D_b^{o*} populations with the n-shells 2-5 most relevant for observation. Redistribution within an n-shell is essentially

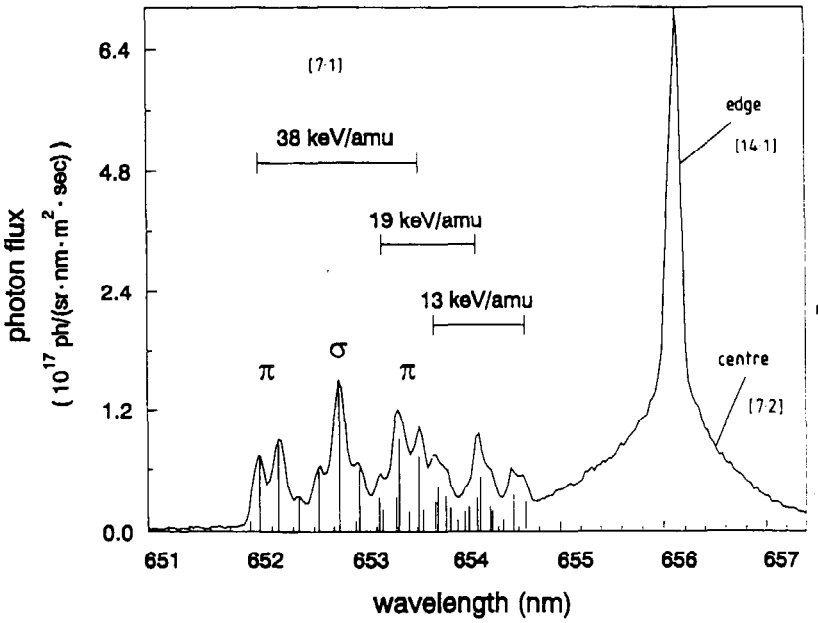

Fig. 8. The deuterium beam emission spectrum. The Stark split beam features are displaced to shorter wavelengths because of the viewing line inclination to the beams. There are three energy components. Edge emission and charge exchange spectroscopy emission make up the whole feature at the natural line position.

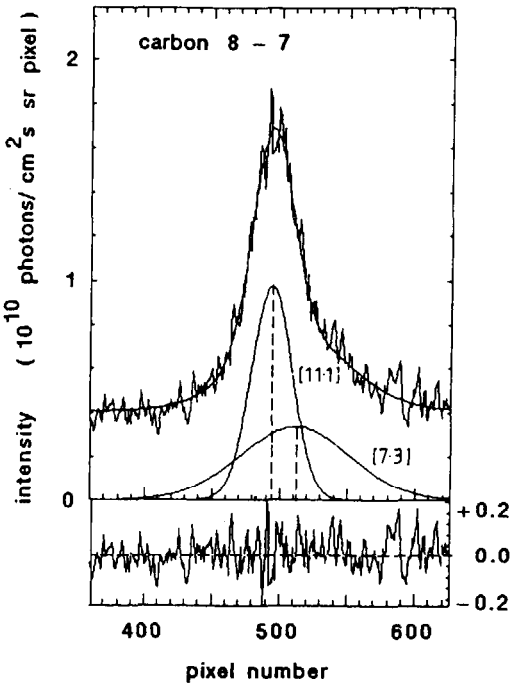

Fig. 9. A typical charge exchange spectroscopy signal in the visible region using deuterium beams. The composite nature of the feature is noted. The narrow edge component and bremsstrahlung backround must be separated by multi-Gaussian fits. Plasma rotation between centre and edge is evident in the components.

complete at $N_e \geq 2x10^{13}$ cm^{-3} and so bundle-n calculations and data are satisfactory for stepwise attenuation corrections and integrated n→n' feature studies. n-shells up to ~12, limited by the field ionisation, need to be included.

At node C2, the same reaction set takes place but with the D^o_{bhp} populations, formed at node C1, and at much lower energies corresponding to plasma thermal temperatures. Electron collisions are relatively more important than ion collisions for ionisation and $\Delta n>0$ excitations. The Stark fields are much smaller and randomly orientated for the D^o_{bhp} atoms (plasma temperatures of 5-20keV are typical) so bundle-n calculations and data are used. Figure 8 shows the Dα beam emission features from the D_b^{o*} population and charge exchange emission from the D^{o*}_{bhp} population. Collectively the D^o_b, D_b^{o*}, D^o_{bhp} and D^{o*}_{bhp} populations provide a complex input to the impurity charge exchange node C3.

b. Helium beams The working diagram for He^0, figure 10, is similar to that for D^0. In particular the helium beam generates a D^o_{bhp} halo population, so that part is not repeated. There is only a single energy beam fraction, but there is a small content of 2^1S and 2^3S metastables which should be included on entry as well as 1^1S. The second line represents these. Since double loss processes occur, there are both He^+_{sb} and He^{+2}_{sb} slowing populations produced at the attenuation node C5. Also at the charge exchange node C6, the double charge transfer

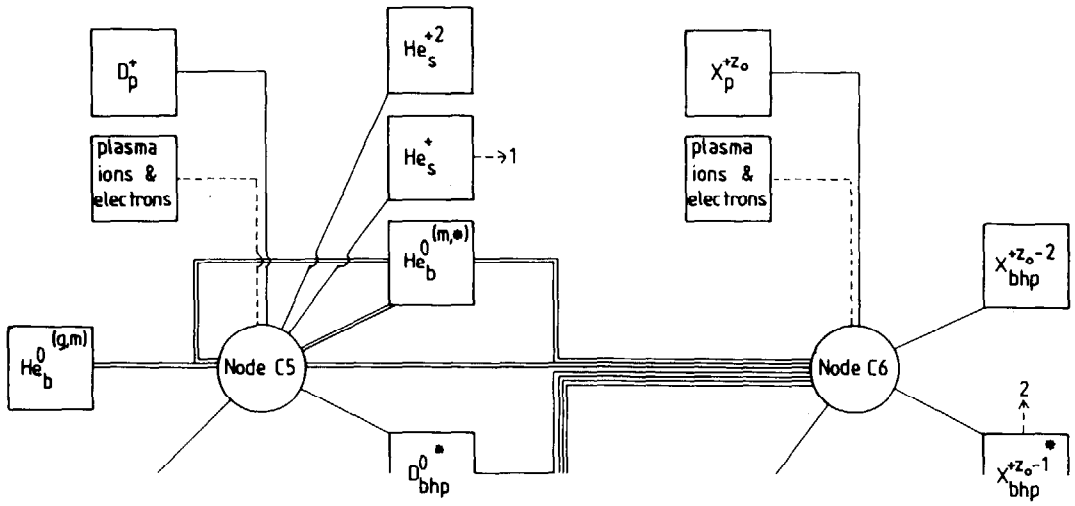

Fig. 10. The working diagram for the reactions in beam emission spectroscopy and charge exchange spectroscopy with helium beams. The slowing populations are noted. The deuterium halo node and charge exchange spectroscopy nodes are not repeated.

reaction is indicated and is of particular relevance for He^{+2} neutralising. The atomic collision data needs in this case have been described recently in some detail (Summers et al., 1992c) and so only a brief summary is given.

Node C5 represents the attenuation reactions. At low density $Ne \leq 5x10^{13} cm^{-3}$ ground state 1^1S loss is the most important, firstly by single electron loss as for D^0 beams.

$$\begin{aligned}
&(\#1)\ He_b^o(1^1S) + D_p^+, X_p^{+z_o} \rightarrow He_{sb}^+ + D_p^+, X_p^{+z_o} + e \quad 10keV \leq E/amu \leq 200keV \\
&(\#1)\ He_b^o(1^1S) + D_p^+, X_p^{+z_o} \rightarrow He_{sb}^+ + D_{bhp}^o, X_{bhp}^{+z_o-1} \quad 10keV \leq E/amu \leq 200keV \\
&(\#1)\ He_b^o(1^1S) + e \rightarrow He_{sb}^+ + e + e \quad 1keV \leq T_e \leq 15keV
\end{aligned} \tag{26}$$

but there are the additional double electron loss processes

$$\begin{aligned}
&(\#2)\ He_b^o(1^1S) + D_p^+, X_p^{+z_o} \rightarrow He_{sb}^{+2} + D_p^+, X_p^{+z_o} + e + e \\
&(\#2)\ He_b^o(1^1S) + D_p^+, X_p^{+z_o} \rightarrow He_{sb}^{+2} + D_{bhp}^o, X_{bhp}^{+z_o-1} + e \\
&(\#2)\ He_b^o(1^1S) + X_p^{+z_o} \rightarrow He_{sb}^{+2} + X_{bhp}^{+z_o-2}
\end{aligned} \tag{27}$$

These reactions and the following reactions are required for the same energy ranges as reactions 26. At densities $\geq 10^{14}$ cm^{-3} and for beam emission spectroscopy, the He_b^{o*} must be established. The reactions include ion impact, which are non-spin changing, and electron collisions. The ground state excitation reactions are

$$\begin{aligned}
&He_b^o(1^1S) + e \rightarrow D_p^+, X_p^{+z_o} \rightarrow He_b^o(n^1L) + D_p^+, X_p^{+z_o} \\
&He_b^o(1^1S) + e \ ③\ He_b^o(n^1L, n^3L) + e
\end{aligned} \tag{28}$$

The redistribution, ionisation and charge exchange reactions involving excited states are

$$\begin{aligned}
&He_b^o(n\ ^{2S+1}L) + D_p^+, X_p^{+z_o} \rightarrow He_b^o(n'\ ^{2S+1}L') + e \\
&He_b^o(n\ ^{2S+1}L) + e \rightarrow He_b^o(n'\ ^{2S'+1}L') + e \\
&He_b^o(n\ ^{2S+1}L) + D_p^+, X_p^{+z_o}, e \rightarrow He_{sb}^+ + D_p^+, X_p^{+z_o}, e + e \\
&He_b^o(n\ ^{2s+1}L) + D_p^+, X_p^{+z_o} \rightarrow He_{sb}^+ + D_{bhp}^o, X_{bhp}^{+z_o-1}
\end{aligned} \tag{29}$$

The n=2 shells are most important (#2 accuracy) for establishing the key metastable populations. Levels up to n=4 need to be maintained in a term resolved picture for beam emission studies (#3 accuracy) but the levels $4<n\leq10$ up to the field ionisation limit may be treated in the bundle-n picture (#4 accuracy). The motional Stark field also effects the He_b^{o*} levels becoming linear at n~4, with associated field mixing, forbidden line emission and alterations in spin system mixing at high l.

c. Lithium beams As described earlier, studies with lithium beams are well established and parallel those for deuterium beams. The atomic reaction sets have been examined in detail by the Vienna group (see Aumayr et al., 1992) and are not repeated here. We remark only the importance of the 2s-2p transition cross-sections and the 2s/2p population ratio in the beam.

2. CHARGE EXCHANGE EMISSION

a. Deuterium beams Although charge exchange as a loss process has been included in the previous subsection, here it is the receiving species which is of concern. The reactions are separated into two nodes (see figure 7) for the initial transfer with fully ionised ions X^{+z_o} and then the details of the X^{+z_o-1} ion which radiates.

At node C3 the primary reactions are the state selective charge transfers from the ground state atoms, D_b^o, in the beam

$$(\#2)\quad D_b^o(1s) + X_p^{+z_o} \rightarrow D_{sb}^+ + X_{bhp}^{+z_o-1}(n\ell) \qquad 5keV \leq E/amu \leq 200keV \tag{30}$$

to which must be added the captures from the thermal halo atoms D_{bhp}^o

$$(\#2)\quad D_{bhp}^o(1s) + X_p^{+z_o} \rightarrow D_p^+ + X_{bhp}^{+z_o-1}(n\ell) \qquad 1keV \leq E/amu \leq 40\ keV \tag{31}$$

The key n-shells are up to $n\sim2z_o^{3/4}$ to allow visible spectroscopy but this has to be extended to $4z_0^{3/4}$ for possible cascading into the key shells. Since the cross-sections to subdominant n-shells decreases as $\sim n^{-3}$ for energies ≥80keV/amu but much more steeply as the collision energy

falls, reactions (31) are usually a small correction ≤10% at $n\sim 2z_0^{3/4}$. Their importance is for the dominant levels $n\sim z_0^{3/4}$. Finally there are the transfers from excited beam and halo atoms.

$$\begin{aligned} &(\#3)\quad D_b^o(n') + X_p^{+z_o} \rightarrow D_{sb}^+ + X_{bhp}^{+z_o-1}(n\ell) && 5\text{keV} \le \text{E/amu} \le 20\text{keV} \\ &(\#3)\quad D_{bhp}^o(n') + X_p^{+z_o} \rightarrow D_{bhp}^+ + X_{bhp}^{+z_o-1}(n\ell) && 1\text{keV} \le \text{E/amu} \le 40\text{keV} \end{aligned} \tag{32}$$

For such transfers, the dominant levels are $n\sim n' z_0^{3/4}$ so they are in principle important for visible spectroscopy, since the cross-sections also scale approximately as n'^4. The charge exchange decreases strongly at energies $\ge 50 n'^2$keV/amu so this counters the large cross-sections for beam donors. The capture is not statistical in substates of the principal quantum shell n. Thus the precise sub-state distribution, which is also modified by redistribution, directly affects the branching ratios for particular line emissions. Models have up to now been in the bundle-nℓj, -nℓ and -n pictures. The ℓ-distribution particularly matters, so cross-section data is needed at least at nℓ-resolution.

Node C4 represents the redistributive and other processes establishing the final $X_{bhp}^{+z_o-1*}$ populations in a collisional-radiative sense. Redistributions within an n-shell are the principle processes at $N_e < 10^{14}$cm^{-3}.

$$(\#2)\quad X_{bhp}^{+z_o-1}(n\ell j) + D_p^+, X_p^{+z_o'}, e \rightarrow X_{bhp}^{z_o-1}(n\ell' j') + D_p^+, X_p^{+z_o'} e \tag{33}$$

These are all thermal collisions. Population mixing by the motional Lorentz field also occurs but a suitable picture within which to model this has not been fully developed. At densities $N_e \ge 10^{14}$ cm^{-3} the further n-shell redistributive and ionisation processes are required.

$$\begin{aligned} &(\#3)\quad X_{bhp}^{+z_o-1}(n\ell j) + e, D_p^+, X_p^{+z_o'} \rightarrow X_{bhp}^{+z_o-1}(n'\ell' j') + e, D_p^+, X_p^{+z_o'} \\ &(\#3)\quad X_{bhp}^{+z_o-1}(n\ell j) + e, D_p^+, X_p^{+z_o'} \rightarrow X_p^{+z_o} + e, D_p^+, X_p^{+z_o'} + e \end{aligned} \tag{34}$$

Electron collisions are the more important here. The excited states formed in the charge exchange capture, radiate quite 'promptly', subject to redistribution + loss, and cascade to the ground state of the $X_{bhp}^{+z_o-1}$ ion. The latter can travel some distance in the plasma, forming a plume along the field lines before being reionised. In the course of this, they can be excited again and radiate giving a 'delayed' emission. This may contribute to observed emission, depending on geometry and ion speeds. Thus the re-excitation reactions for completeness (from the ground state) are

$$(\#3)\ X_{bhp}^{+z_o-1}(1s)+e \rightarrow X_{bhp}^{+z_o-1}(n\ell j)+e$$
$$(\#3)\ X_{bhp}^{+z_o-1}(1s)+e \rightarrow X_{p}^{+z_o}+e+e \qquad (35)$$

with electron collisions only important. The relevant species X^{+z_o} are the light impurity list.

b. Helium beams The difference with deuterium beams occurs at node C6 in figure 10. The redistributive node C4 is identical. The 2^1S and 2^3S metastables in helium beams have substantially higher populations than the excited n=2 shell in deuterium beams.

At node C6, the primary reactions are

$$\begin{aligned}
&(\#2)\ He_b^o(1^1S)+X_p^{+z_o} \rightarrow He_{sb}^{+}+X_{bhp}^{+z_o-1}(n\ell) && 5keV \le E/amu \le 200keV\\
&(\#2)\ He_b^o(1^1S)+X_p^{+z_o} \rightarrow He_{sb}^{+2}+X_{bhp}^{+z_o-1}(n\ell)+e && (36)\\
&(\#2)\ He_b^o(2^1S,2^3S)+X_p^{+z_o} \rightarrow He_{sb}^{+}+X_{bhp}^{+z_o-1}(n\ell)\\
&(\#2)\ He_b^o(1^1S)+X_p^{+z_o} \rightarrow He_{sb}^{+2}+X_{bhp}^{+z_o-2}
\end{aligned}$$

The state selective charge transfer to subdominant impurity levels from the ground state appear to be substantially smaller than for deuterium beams. Thus the metastables play a potentially much more important role for charge exchange spectroscopy with helium beams. Halo contributions, that is from D_{bhp}^o donor remains the same. Finally the double charge transfer reaction is noted since it allows neutralised helium escape from the plasma. This is important when there are fast He^{+2} populations in the plasma such as from deuterium-tritium fusion (see section E).

D. THE EDGE, SCRAPE-OFF -LAYER AND DIVERTOR PLASMA

The last closed flux surface has been identified as a key position in the fusion plasma. Within it, the ideal magnetic flux surfaces are closed and the plasma is confined, while outside in the SOL particles flow along magnetic field lines to sinks at their connection points with solid surfaces. For the confined plasma, anomalous (transverse) diffusion of particles and heat from flux surface to flux surface is the main concern. In the SOL, parallel particle and conductive fluxes to the sinks, matched to the particle and heat flux across the last closed flux surface from the bulk plasma, determine the primary characteristics of the SOL. Typical density and temperature e-folding lengths are ~1-2cm (midplane in JET single null X-point operation). The detailed kinetic description of electron and ion flows to the connected surfaces establish the surface sheath and longitudinal electric fields in the SOL (Stangeby & McCracken, 1990). The

flux, terminal speeds (M=1) and incidence angles of deuterons and impurity ions, accelerated by these fields, on the contact surfaces determine the sputtering and release of impurities back into the plasma (i.e. the sources). Passage of neutral particles from wall and limiter sources through the SOL is relevant. Ionisation of neutral particles within the SOL leads to their entrapment and 'screening' from the bulk plasma.

The direction of attempts to control impurities in the presence of the very large fluxes of particles and energy into the SOL centre on the axisymmetric poloidal 'divertor'. By creation of a poloidal magnetic null within the plasma volume at the top or bottom of the vessel, the position of the separatrix allows the inner and outer arms of the SOL to be led into a divertor remote from the bulk plasma. The strike zones on the divertor target plates are the only direct plasma/surface contacts. Pumped divertor design seeks to establish plasma flow towards the divertor. In principle, the frictional force associated with this flow counters the thermal gradient force tending to move impurities towards the bulk plasma (Keilhacker et al., 1991). This retains impurities in the divertor. Further, with long connection lengths and high density in the SOL, a strongly radiating low temperature ($T_e \leq 10eV$) high density ($N_e \geq 10^{14} cm^{-3}$) divertor plasma may be obtained, reducing conducted flux to the target plates and minimising sputtering. Choices of divertor target species, together with gas introduction at the separatrix are aspects of the impurity control. Broadly the types of cross-section data are equivalent to those in the high temperature plasma except that low states of ionisation matter, the ionisation state is dynamic and the density is high in relation to the ionisation state (c.f. N_e/z^7).

A major difference is the high concentration of neutral deuterium. It is present in the SOL/divertor plasma because of recycling from the strike zones or other surfaces contacted by the plasma and charge exchange neutrals. There may also be heavy gas puffing (Gondhalekar et al., 1990). In equilibrium, the D^+ flux to the surface is equal to the D^0 release (a recycling coefficient of unity). The release may be backscattered D^0, molecular D_2, or compounds such as CD_4 with carbon composite targets. The D_2 and CD spectra are commonly observed in tokamak divertors reflecting a catabolic chemistry leading ultimately to D^0 (Behringer, 1990; Prospieszczyk et al, 1987). In interpreting spectral emission such as $D\alpha$, molecular precursors are of concern both for the velocity population groups contributing to the spectral profile and for direct population of the excited state. However such molecular processes occur very close to the surface sources. The first concern is the exceptional diffusion of the D^0 atom due to charge exchange with thermal plasma D^+, producing a higher kinetic energy second generation neutral. There may be several charge exchange reactions before ionisation. Equally this process allows formation of fast neutrals which can penetrate the SOL to impact vessel walls (see Harrison (1985) for an overview). Divertor studies in JET seem to indicate substantial unexpected wall sources probably due to such processes (Matthews, 1992). The net result is a D^0 layer extending ~10-20cm into the plasma compared with the 2-3mm for other neutral species. Collision data needs for D^0 relate to measurement of its flux, density dependent line ratios and

its role as a charge exchange donor to impurities. The main spectral observations are of the Balmer-series up to n=6, in the visible, some Paschen members in the infrared and Lyman α and β in the VUV. The density sensitive ratios arise from collisional depopulation of the higher n-shells, D^0 is very much in the collisional-radiative regime in divertors conditions. It should be added that the optical depth question for Lyman lines of D^0 in the divertors appears not to have been addressed, although estimates clearly indicate its importance. The consequent disturbance of the D(n=2) population must be carried into 'thermal' charge exchange spectroscopy.

Major attention must be directed to neutral impurity species since they can be directly associated with the surfaces from which they are released. They move short distances, independent of magnetic field (ionisation lengths ~2-3mm) to their point of first ionisation and provide the most immediate information on impurity sources, influx, sputtering yield etc. Firstly we are concerned with the light impurities, especially Be, B, C, O. They all have metastable states in the n=2 complex with uncertain and variable population proportions, depending on released state and the local highly ionising environment. Electron collisions are responsible, for their excitation and ionisation (Behringer et al., 1989). Preferred spectral observations of such localised emitters are in the visible and quartz UV. This and the need for sufficient spectral lines which can be related to all the metastables requires transitions from up to the n=4 shell. Primary observations for carbon include CI($2s2p^2(^4P)3p\ ^3P$ - $2s2p^2(^4P)3s\ ^3P$) and for beryllium include BeI($2s3s\ ^1S$ - $2s2p\ ^1P$) and BeI($2s4s\ ^1S$ - $2s2p\ ^1P$). There is substantial redistribution and reionisation involving the n =4 and 3 shells. The full generalised-collisional radiative picture is appropriate (Summers et al., 1992b). This presents a substantial cross-section data need which refined calculations are only beginning to be able to provide. Secondly there are the heavier neutrals including transition metals such as Cr, Fe and Ni. They may be regarded as typical of the complexities presented by heavier species. Transition metals have electron configurations of the form $3p^63d^q$, $3p^63d^{q-1}4s$, $3p^63d^{q-2}4s^2$ which provide the ground state and many metastable states. Metastables of high statistical weight exist and the degree to which they are populated in the inflowing neutrals is a matter of importance but as yet unclear. Studies of similar, but ionic systems (Fe^{+2}, Fe^{+3}) in translational energy loss spectroscopy of charge exchange indicate a complex mixture of initial populated states from ECR sources (Gilbody, 1993). This means that measurement of one of two spectrum lines of such a neutral may be insufficient to allow deduction of fluxes. On the other hand, the lowest resonance lines of such systems, of the form $3p^63d^{q-1}4s$-$3p^63d^{q-1}4p$ and $3p^63d^{q-2}4s^2$-$3p^63d^{q-2}4s4p$ tend to occur in the visible and quartz UV ranges. Parentage breakdown is severe and so association of line with metastable proves difficult. Evidently the collision data need is very real here. Comprehensive cross-section calculations between the configurations indicated above together with ionisation cross-sections for the various metastables would allow computation of the coupled photon efficiencies and so let diagnostic studies progress.

1. IMPURITY EMISSION AND THE INFLUENCE OF NEUTRAL DEUTERIUM.

The working diagram for reactions of impurities in this region is given in figure 11. It is similar to figure 4 of section B, but draws special attention to charge exchange recombination with neutral deuterium through a new node D1. The deuterium and impurity atoms and ions are given the subscripts 'edp' for edge divertor plasma emphasising their complex velocity distributions. Kinetic energy at release is not immediately equilibrated with the thermal plasma but is achieved over a few ionisation lengths. This is reflected in the profiles of spectrum lines from the various ions. Basic modelling for deuterium includes at least two kinetic populations, that of initial release and the thermalised one achieved through charge exchange reactions. These are indicated by the two entrant lines to node D1, for the ground state and

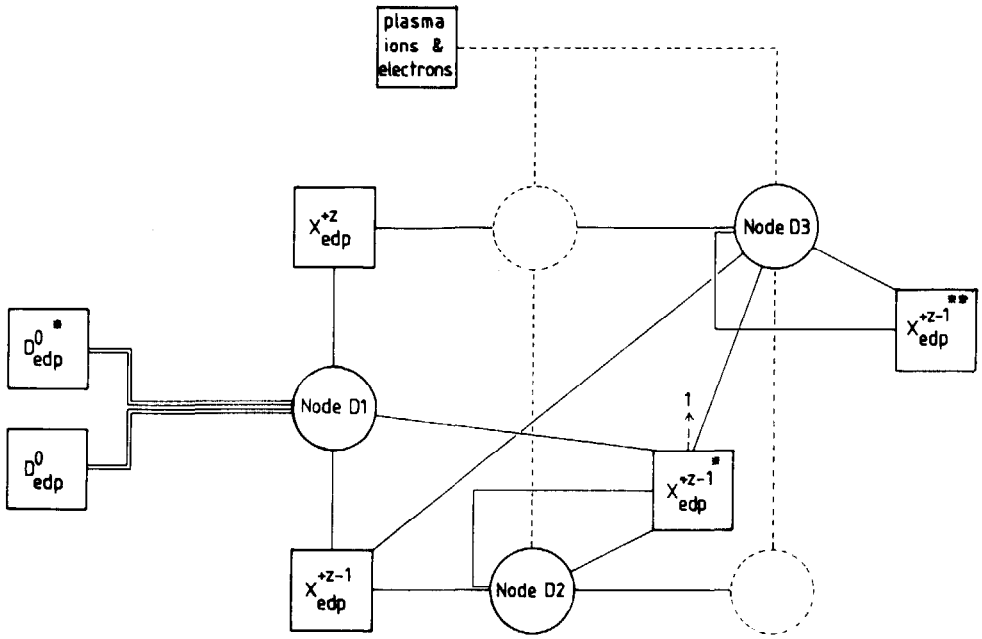

Fig. 11. Working diagram for edge impurity populations and reaction nodes including the influence of neutral deuterium on recombination.

excited states. Evidently this is a simplification.

At node D1, the charge transfer reactions with impurity ions are

$$\begin{aligned} &(\#2)\quad D^{o}_{edp}(1s)+X^{+z}_{edp}(\rho) \rightarrow D^{+}_{edp}+X^{+z-1}(\rho_{-}) \\ &(\#2)\quad D^{o}_{edp}(1s)+X^{+z}_{edp}(\rho) \rightarrow D^{+}_{edp}+X^{+z-1}((\sigma)n\ell SL) \end{aligned} \tag{37}$$

The first alters the state of ionisation without generating prompt cascade radiation. These captures are a substantial part of the total for light near neutral ions. The second gives such emission as well as contibuting to the effective overall recombination. Since ionisation

from excited states and redistributive collisions occur even at the n=3 shell in such ions, the excited population following the charge transfer must enter the collisional-radiative loop at node D2 for proper evaluation of the generalised collisional radiative recombination coefficients. The charge exchange reactions are strongly state selective at the low particle impact energies at the plasma edge. Typically only three or four states are involved, also these can include excitation with transfer cases so the alteration of parent $\rho \rightarrow \sigma$ is noted. Reaction rates must be averages over the kinetic distribution functions of both reactants and so a description of the cross-sections from threshold to about 100eV/amu in the relative frame is required. The captures from the deuterium ground state generally contrbute to VUV emission. However spectrum lines, including visible lines, from highly excited states are observed, suggestive of charge exchange reactions. These are

$$(\#3) \quad D^{o}_{edp}(n=2,3) + X^{+z}_{edp}(\rho) \rightarrow D^{+}_{edp} + X^{+z-1}_{bhp}((\rho)nl[SL]) \tag{38}$$

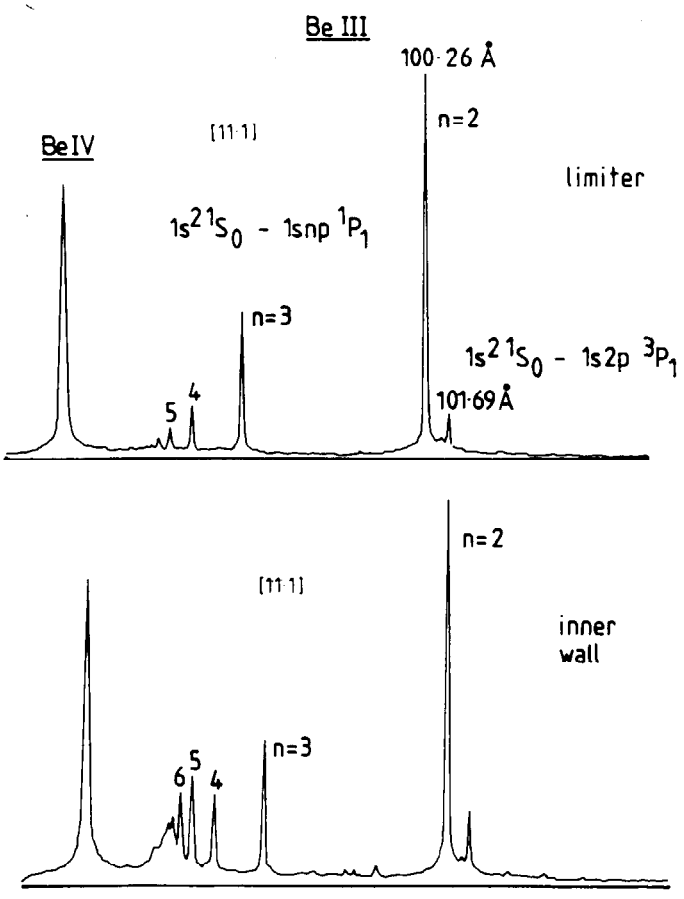

Fig. 12. Be XUV spectrum lines showing modification of the series decrement when the plasma moves into contact with the inner wall. This indicates charge transfer reactions from excited deuterium near the wall.

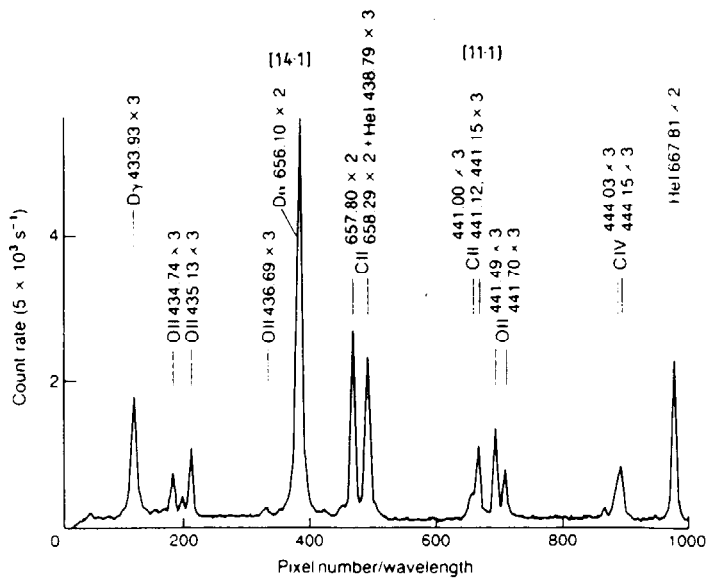

Fig. 13. Visible spectrum showing influx ions from limiters in JET helium plasmas. 2nd. and 3rd. order spectra are present. The spectral region is well suited to assessment of sputtering yields relative to D or He.

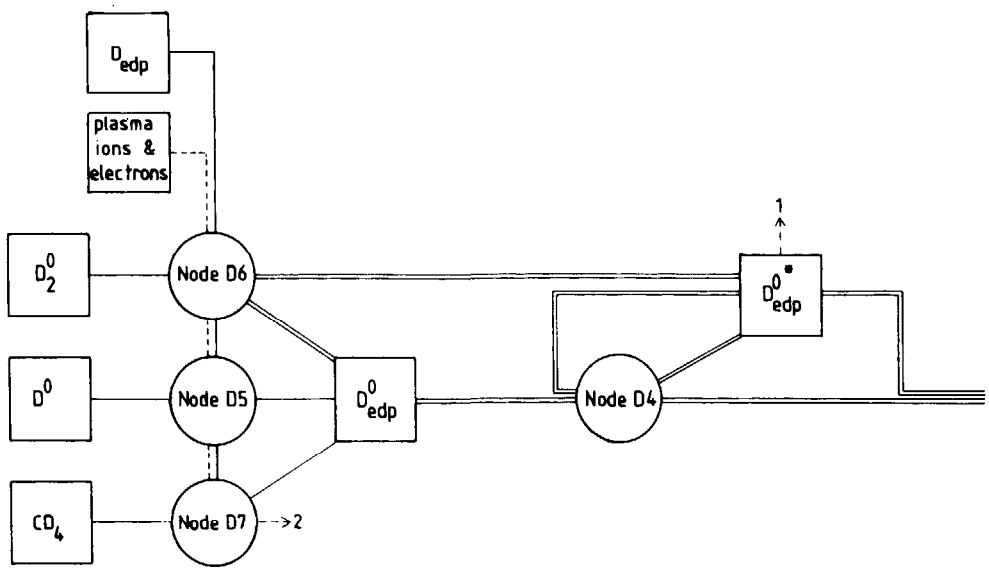

Fig. 14. Working diagram for establishing neutral deuterium ground and excited populations from molecular and atomic sources.

with n=3,4,..... These reactions are again quite strongly n-shell selective, approximately at the resonant n-shell. Captures by light bare nuclei and helium-like ions from the excited states of deuterium contribute to the overlapping edge emission within the charge exchange spectroscopy signals driven by the neutral beams.

At node D2, the excited populations formed by charge transfer enter along with those formed by electron impact excitation and those formed by free electron recombination. The excitation part is most important for the inflowing light ions and diagnostic spectroscopy. It is similar to that described for node B1, but accurate cross-sections with higher n-shells at full resolution are required for the light element ions. The essential reactions are

$$\begin{aligned} &(\#2)\ X^{+z-1}_{edp}(\rho_-)+e \rightarrow X^{+z-1}_{edp}((\rho)nlSL)+e \qquad 2\le n\le 4 \\ &(\#3)\ X^{+z-1}_{edp}((\rho)nlSL)+e \rightarrow X^{+z-1}_{edp}((\sigma)n'\,l'\,S'\,L')+e \end{aligned} \tag{39}$$

for $2\le z_0\le 8$ and $1\le z\le 7$. It is Maxwell averaged rates from 0.5eV - 100eV which are used in practice. The collisional mixing processes described in the second reaction are quite strong and also the connection to higher less resolved n-shells is necessary to obtain proper coupling through stepwise excitation to the continuum and ionisation. The collision limit for the neutral light atoms is at n~4-5 in the edge -divertor plasma.

The reactions are

$$\begin{aligned} &(\#4)\ X^{+z-1}_{edp}((\rho)nlSL)+e \rightarrow X^{+z-1}_{edp}((\rho)n'[l'])+e \qquad n'>4 \\ &(\#4)\ X^{+z-1}_{edp}((\rho)n[l])+e \rightarrow X^{+z-1}_{edp}((\rho)n'[l'])+e \qquad n,n'>4 \end{aligned} \tag{40}$$

The ionisation and recombination reactions are as described for nodes B1 and B3 but adjusted to the higher resolution levels at higher n-shells

For medium to heavy metals, the completeness sought for the light elements cannot reasonably be matched either experimentally or theoretically at present.

2. RECYCLING DEUTERIUM AND MOLECULAR ASPECTS

The final diagram, figure 14, is for establishing the populations D^0_{edp} and D^{0*}_{edp} in the edge and divertor regions. These are the effective deuterium sources for the reactions with impurities in diagram 11.

Node D4 represents the reactions causing excitation of $D^0(1s)$. At plasma densities $N_e \sim 10^{12} - 10^{14}$ cm^{-3}, nearly degenerate states of the same principal quantum shell are relatively statistically populated so only the bundle-n data is required.

$$(\#2)\quad D^o_{edp}(n)+e \rightarrow D^o_{edp}(n')+e \qquad 1\le n<n'\le 6 \qquad (41)$$

$$(\#2)\quad D^o_{edp}(n)+e \rightarrow D^+_{edp}+e+e$$

Surprisingly, it has been difficult to be confident of such cross-section data for excitation from n=1 to n≥3 at energies ~ 13 - 20 eV. Recombination data for D^0 is well known but it is the ionising environment which matters most here. Redistribution in n through charge transfer with deuterons is often omitted on the grounds that the most likely transfer is to the same n-shell. In fact there is a modest redistribution in n-shell even at low energy

$$(\#3)\quad D^o_{edp}(n)+D^+_{edp} \rightarrow D^+_{edp}+D^o_{edp}(n') \qquad (42)$$

The collisional-radiative calculation for deuterium excited populations at node D4 is the ancestor of all the more elaborate collisional-radiative calculations and is certainly necessary at the present temperatures and densities. The radiation field has not been addressed yet. However atomic deuterium and its emission cannot be treated in isolation from its source and it is these connections which require most attention. We have represented these connections by nodes D5, D6 and D7, which are simplifications. It enters the area of plasma chemistry which is developed in detail in another work in this volume.

At node D5, the concern is the penetration of neutral atoms from a surface source into the plasma. The key reactions are

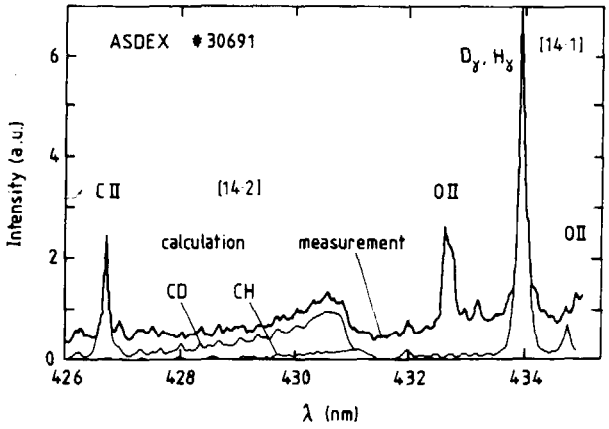

Fig. 15. Spectrum from the ASDEX tokamak showing the CH and CD molecular bands. (Behringer, 1990)

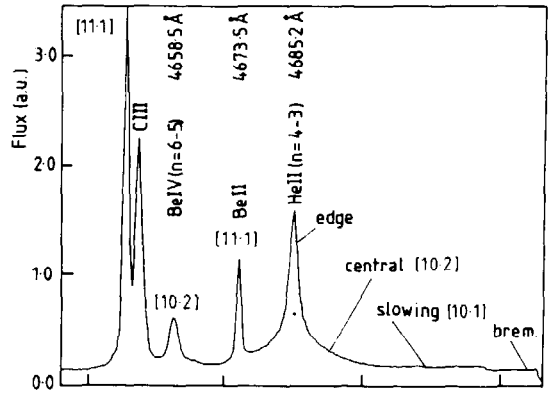

Fig. 16. Slowing down spectrum for helium as revealed in charge exchange spectroscopy with helium beams.

$$(\#2)\quad D^{o}(1s)+D^{+}_{edp} \rightarrow D^{+}_{edp}+D^{o}_{edp}(1s)$$

$$(\#2)\quad D^{o}(1s)+e \rightarrow D^{+}_{edp}+e+e \qquad (43)$$

E SPECIAL POPULATIONS

1. SLOWING DOWN POPULATIONS

The populations D^{+}_{sb}, He^{+1}_{sb} and He^{+2}_{sb} resulting from ionisation of neutral beams have been introduced in section C. Having beam energy at birth, they slow down initially by collisions with electrons, finally scattering and thermalising with the background plasma ions. The bare nuclei travel substantial distances before this occurs so the population distributions extend throughout the plasma volume although constrained in movement across flux surfaces. The He^{+}_{sb} ions are lost by ionisation but still travel a significant distance before this occurs, forming an extended plume. A key population in the future 'active' phase of the fusion programme is the alpha particles formed by D-T fusion. Their population is analogous to the He^{+2}_{sb} population but born at 880 keV/amu. The source rate, slowing and confinement of this population are crucial matters for fusion. Present fusion devices already produce a similar population during ion cyclotron resonance heating (ICRH) coupled through seeded minority species $^{3}He^{+2}$ or $^{4}He^{+2}$. These ions are accelerated to energies ~ 1MeV at the absorbing layer, slowing down as they diffuse away from the layer.

Measurements on these alpha particle populations require firstly double or single charge transfer from a suitable donor. In the former case, the neutralised He^0 atom can escape from the plasma volume, subject to some attenuation from its source to the plasma periphery, where energies and count rates can be analysed. The collision data for the attenuation has been identified in section C.1.b, although they must be extended in energy range from 100 keV/amu to 880 keV/amu. Neutralising by He^0 beams is proposed for ITER (reaction 29(3)). More details of the cross-section status and needs for alpha particle detection are given in the special issue - Nuclear Fusion Supple, (1992) Vol 3 (see Summers et al. (1992c) for the overview). Lithium pellet injection is also suggested for alpha particle neutralisation. Single charge transfer forming the He^+ population using neutral deuterium or helium beam donors is the proposed charge exchange spectroscopy route to alpha particle measurement. With beam particle energies ≤ 80 keV/amu, substantially slowed alpha particles of energies ≤200 keV/amu only are detected. The emission features are expected to be broad (restricted by the cross-section fall-off with energy) and asymmetric (von Hellermann et al., 1991, 1993). Figure 16 illustrates a slowing feature, but with a beam particle origin. The interpretation of such features is complex, since thermal neutral deuterium at the plasma periphery can act as a donor to recombining He^{+2} as well as the beam donor; also the beam atom plume as it ionises through He^+ can contribute. A full study of the He^+ slowing populations requires the reactions 33 and 34 of section C.2.a with the ion collisions of greater weight because of the higher energy collisions. Also reactions 35 must be extended to include

$$(\#2)\quad He^+(1s) + D^+, X^{+z'_o} \rightarrow He^{+2} + D^+, X^{+z'_o} + e$$

$$(\#2)\quad He^+(1s) + X^{+z'_o} \rightarrow He^{+2} + X^{+z'_o-1} \qquad \text{E/amu} \le 880\ \text{keV} \qquad (44)$$

Finally, neutralising of fast, slowing H^+ populations formed in ICRH must be mentioned. The relatively high energy of H^0 atoms detected by neutral particle analysis and the similarity of the energy dependence with and without neutral beams (the absolute signal levels are much enhanced with neutral beams present) (Gondhalekar et al., 1993) suggest that heavier species such as C^{+5} may be acting as intermediaries. That is charge transfer from D^0 beams to C^{+6} plasma ions and then transfer from C^{+5} to fast H^+ may occur. This indicates that the reactions

$$(\#2)\quad H^+ + X^{+z'_o-1} \rightarrow H + X^{+z'_o} \qquad 4 \le z_0 \le 8\ ,\ \text{E/amu} \le 1\ \text{MeV} \qquad (45)$$

should be included in the studies.

2. MARFES

To conclude, we mention an example of erratic phenomena in fusion plasma where atomic processes are prominent. Marfes (multifaceted asymmetic radiation from the edge) were first observed on ALCATOR C (Lipschultz et al., 1984). In JET, a marfe can form as a strongly radiating zone close to the upper X-point strike points in divertor-like operation. It may move, oscillating between the X-point and midplane down the inner vessel wall. The marfe can radiate a substantial part of the input power, particularly giving anomalous radiation excess in the VUV around 120-160Å. It appears to be a high density, low temperature condensation arising from a radiative thermal instability (Stringer, 1985). The specific radiating ions, the interaction with the vessel wall and the transient ionisation state character of the marfe have not been clearly established. Low ionisation stages of nickel emitting a dense VUV line spectrum in a recombining environment may contribute. Analysis of such problems draws heavily on reaction cross-section data of the type descibed in sections B and D. Extensive complex ion 'specific ion files' are prepared and processed using the collisional-radiative models of section A leading finally to spectral syntheses and the confrontation with the spectral measurement.

F CONCLUSIONS

In describing the collision cross-section data needs for the present and future fusion programme, attention has been drawn to some of the actual practical difficulties of bringing the manifestly huge volume of available data into effective use in large fusion establishments. There, the disparate requirements of many applications form spectroscopic diagnostics through to purely theoretical plasma simulations must be balanced and consistent sources and qualities maintained. For these reasons, emphasis has been placed on management of data and on a modelling approach, generalised collisional radiative theory, which can ensure this.

Then, we have examined the needs in the three primary areas. It is in these areas, particularly in beam penetrated plasma and divertor plasma, that strong continued development is anticipated over the next few years. and for which new and refined cross-section data is essential. We have sought to identify the reactants, classes of cross-sections, resolutions and broad precisions which are required and how they fit into the overall modelling picture.

The hope and belief is that the high quality atomic collision data which can now be generated routinely, systematically produced, organised and merged with the more sophisticated utilisation structures can now establish a new standard of reliability and usefulness of 'atomic modelling for fusion' sufficient to support the fusion programme through to ignition and a demonstration reactor.

G REFERENCES

Aumayr, F., Schorn, R.P., Pockl, M. et al. (1992) J. Nucl. Mater. 196-198, 928.

Bates, D.R., Kingston, A.E. and McWhirter, R.W.P. (1962) Proc. Roy. Soc A267, 297.

Barnett, C.F. (1990) Editor-Atomic Data for Fusion Vol I, ORNL-6086/V1.

Behringer, K. (1987) JET Joint Undertaking Report JET-R(87)08.

Behringer, K. (1990) J. Nucl. Mater. 176-177, 606.

Behringer, K., Summers, H.P., Denne, B. et al., (1989) Plasma Phys. Control. Fusion 31, 2059.

Bitter, M., Hill, K.W., Zarnstorff, M. (1985) Phys. Rev. A32, 3011.

Bitter, M., Hsuan, H., Decaux, V. et al. (1991) Phys. Rev. A. 44, 1796.

Boileau, A., von Hellermann, M., Horton, L.D. and Summers, H.P. (1989a) Plasma Phys. Control. Fusion 31, 779.

Boileau, A., von Hellermann, M., Mandl, W. et al. , (1989b) J. Phys. B. 22, L145.

Bombarda, F., Giannella, R., Kallne, E. et al. (1988) Phys. Rev. A 37, 504.

Burgess, A. (1965) Astrophys. J. 141, 1588.

Burgess, A. and Tully, J.A. (1992) Astron. & Astrophys. 254, 436.

Burgess, A. and Summers, H.P. (1976) Mon. Not. R. Astr. Soc. 174, 345.

Burgess, A. and Summers, H.P. (1987) Mon. Not. R. Astr. Soc. 226, 257.

Burrell, K.H., Allen, S.L., Bramson, G. et al. (1989) Plasma Phys. Control. Fusion 31, 1649.

Costley, A.E. (1991) 'Diagnostics for Contemporary Fusion Devices' p223 (Int. School of Plasma Phys., Varenna - ed. Stott, P.E.; publ.-Societa Italiana de Fisica)

Danielsson, M., von Hellermann, M.G., Kallne, E. et al. (1992) Rev. Sci. Instr. 63, 2241.

de Michelis, C. and Mattioli, M. (1984) Rep. Prog. Phys. 47, 1233.

Denne, B., Hinnov, E., Ramette, J. et al. (1989) Phys. Rev. A 40, 1488.

Denne-Hinnov, B., Lauro-Taroni, L., Giannella, R. et al. (1993) Plasma Phys. Control. Fusion - to be submitted.

Fonck, R.J., Goldston, R.J., Kaita, R. and Post, D.E. (1983) Appl. Phys. Lett. 42, 239.

Fonck, R.J., Darrow, D.S. and Jaehnig, R.P. (1984) Phys. Rev. A. 29, 3288.

Giannella, R., Behringer, K., Denne, B. et al. (1989) Proc. 16th Europ. Conf. on Control. Fusion and Plasma Physics, Venice, Italy, vol. 13B, 209.

Gilbody, H.B. (1993) Proc. IAEA Special Meeting on the Atom., Molec. and Surface Interact. Data Needs for ITER, (Oct. 1992), Cadarache, France (ed. - Janev, R.K.; publ. - Elsevier).

Gilbody, H.B., Dunn, K.F., Browning, R. et al. (1971) J. Phys. B 4, 800.

Gondhalekar, A., Erents, S.K., Morgan, P.D. et al. (1990) J. Nucl. Mater. 176-177, 600.

Gondhalekar, A., Corti, S., Khudoleev, A.V. et al. (1993) Nucl. Fusion - to be published.

Gowers, C. (1991) 'Diagnostics for Contemporary Fusion Devices' p261 (Int. School of Plasma Phys., Varenna - ed. Stott, P.E.; publ.-Societa Italiana de Fisica)

Groebner, R.J., Brooks, N.H., Burrell, K.H. and Rottler, L. (1983) Appl. Phys. Lett. 43, 920.

Harrison, M.F.A. (1985) Culham Laboratory Report CLM-P746.

Hemsworth, R. and Traynor, N. (1990) JET Joint Undertaking Internal Report JET-DN(90) 86.

Hirooka, Y., Conn, R.W., Sketchley, T. et al. (1990) J. Vac. Sci. Technol. A8, 1790

Hirooka, Y. and the PISCES team (1991) UCLA Inst. Plasma Fusion Research Progress Report UCLA-PPG#1380.

Hoekstra, R., de Heer, F.J. and Morgenstern, R. (1991) - private communication (to be published)

Hulse, R. A. (1983) Nucl. Tech./Fusion 3, 259.

Isler, R.C. (1981) Phys. Rev. 24, 2701.

Jaeckel, H.J., Lingertat, J., Summers, D.D.R. et al. (1992) Proc. 19th Europ. Conf. on Control. Fusion and Plasma Physics, Innsbruck, Austria, VolII, p727.

Keen, B.E. and the JET team (1991) JET Joint Undertaking Progress Report 1991, EUR 14434 EN (EUR-JET-PR9).

Keen, B.E., Watkins, M.L. and the JET team (1992) Europhys. News 23, 123.

Keenan, F.P. and Reid, R.H.G. (1989) Physica Scripta 39, 314.

Keilhacker, M., Simonini, R., Taroni, A. and Watkins, M.L. (1991) Nuclear Fusion 31, 535.

Lawson, K.D. and Peacock, N. J. (1992) JET Joint Undertaking Technical note TAN(92)1-5.

Lipschultz, B., LaBombard, B., Marmar, E.S. et al. (1984) Nuclear Fusion 24, 977.

Lotz, W. (1967) Astrophys. J. Supple 14, 207.

McWhirter, R.W.P. and Summers, H.P. (1984) 'Applied Atomic Collision Physics' vol 2, ch. 3 (ed. Massey, H.S.W.; publ. - Acad. Press, New York).

Mandl, W., Wolf, R.C., Von Hellermann, M.G. et al. (1993) Plasma Phys. Control. Fusion - in press.

Matthews, G. Stangeby, P.C., Elder, J.D. et al. (1992) J. Nucl. Materials 196-198, 374.

McCormick, K.(1986)Proc. Summer School on 'Basic and Advanced Diagnostic Techniques for Fusion Plasmas', Varenna, Italy, p635.

McCullough, R.E., Goffe, T.V. and Gilbody, H.B. (1978) J.Phys.B. 11, 2333.

May, M.J., Zwicker, A.P., Moos, A.W. (1992) Rev. Sci. Instrum. 63, 5176.

Pasini, D., Mattioli, M., Edwards, A.W. et al. (1990) Nucl. Fusion 30, 2049.

Pasini, D., Gill, R.D., Holm, J. et al. (1988) Rev. Sci. Instrum. 59, 693.

Paul. S.F. and Fonck, R.J. (1990) Rev. Sci. Instrum. 61, 3496.

Post, D.E., Jensen, R.V., Tarter, C.B. et al. (1977) At. Data. Nucl. Data Tables 20, 397.

Prospieszczyk, A., Bay, H.L., Bogen, P. et al (1987) J. Nucl. Mater. 145-147, 574.

Sato, K., Suckewer, S. and Wouters, A (1987) Princeton Plasma Physics Lab. Rep. PPPL-2449.

Schorn, R.P., Claassen, H.A., Hintz, E. et al. (1991) Proc. 18th. Europ. Conf. Control. Fusion & Plasma Physics, vol.III, 125.

Seaton, M.J. (1964) Planet. Space Sci. 12, 55.

Stangeby, P.C. and McCracken, G.M. (1990) Nucl. Fusion 30, 1225.

Stott, P.E. (1992) Rep. Prog. Phys. 55, 1715.

Stratton, B.C., Ramsay, A.T., Boody, F.P. (1987) Nucl. Fusion 27, 1147.

Stringer, T.E. (1985) Proc. 12th Europ. Conf. on Control. Fusion and Plasma Physics Vol97, p86

Summers, H.P. (1977) Mon. Not. R. Astr. Soc. 178, 101.

Summers, H.P. and Dickson (1992a) 'Recombination of Atomic Ions' ,NATO Advanced Study Institute series, vol 296, p31 (ed. W.G. Graham - publ. Plenum Press, New York).

Summers, H.P., Dickson, W.J., Boileau, A et al., (1992b) Plasma Phys. Control. Fusion 34, 325.

Summers, H.P., Giannella, R., von Hellermann, M. (1990) 'Atomic Spectra and Oscillator Strengths', p211 (ed. Hanson, J.E.; publ.-North Holland).

Summers, H.P. and Hooper, M.B. (1983) Plasma Phys. Control. Fusion 25, 1311.

Summers, H.P., von Hellermann, M., Breger, P. et al. (1991) Amer. Inst. Phys. Conf. Proc. 251, 111.

Summers, H.P., Von Hellermann, de Heer, F.J. and Hoekstra, R,. (1992c) Nucl. Fusion Supple., At. & Plasma Mater. Inter. Data for Fusion 3, 7.

Summers, H.P. and Wood, L. (1988) JET Joint Undertaking Report, JET-R(88)06.

Tanga, A., Behringer, K.H., Costley, A.E. et al. (1987) Nucl. Fusion 27, 1877.

Thomas, P.R. (1990) J. Nucl. Materials 176-177, 3.

Tobita, K., Itoh, T., Sakasai, A. et al . (1990) Plasma Phys. Control. Fusion 32, 429.

Tombabechi, K. and the ITER conceptual design team (1991) ITER docum. series no 18. IAEA/ITER/DS/18, IAEA, Vienna.

van Regemorter, H. (1962) Astrophys. J. 136, 906.

von Hellermann, M.G. and Summers, H.P. (1992) Rev. Sci. Instr. 63, 5132

von Hellermann, M.G., Mandl, W.,et al. (1991) Plasma Phys. Control. Fusion 33, 1805

von Hellermann, M.G., Core, W.G.F., Frieling, J. et al. (1993) Plasma Phys. Control. Fusion - in press.

Wagner, F., Becker, G., Behringer, K. et al. (1982) Phys. Rev. Lett. 49, 1408.

Wesson, J. (1987) 'Tokamaks' ,Oxford Engineering Science series; no. 20 (publ.-Clarendon Press, Oxford).

Wroblewski, D., Burrell, K.H., Lao, L.L. et al. (1990) Rev. Sci. Instrum. 61, 3552.

Zastrow, K.-D., Kallne, E. and Summers, H.P. (1990) Phys. Rev. A41, 1427.